EHD2 regulates caveolar dynamics via ATP-driven targeting and oligomerization

Björn Morén[a], Claudio Shah[b], Mark T. Howes[c], Nicole L. Schieber[c], Harvey T. McMahon[d], Robert G. Parton[c], Oliver Daumke[b], and Richard Lundmark[a]

[a]Medical Biochemistry and Biophysics, Laboratory for Molecular Infection Medicine, Sweden, Umeå University, 901 87 Umeå, Sweden; [b]Max Delbrück Center for Molecular Medicine, Crystallography, 13125 Berlin, Germany; [c]Institute for Molecular Bioscience and Centre for Microscopy and Microanalysis, University of Queensland, Brisbane, Queensland 4072, Australia; [d]MRC Laboratory of Molecular Biology, Cambridge CB2 0QH, United Kingdom

ABSTRACT **Eps15 homology domain–containing 2 (EHD2) belongs to the EHD-containing protein family of dynamin-related ATPases involved in membrane remodeling in the endosomal system. EHD2 dimers oligomerize into rings on highly curved membranes, resulting in stimulation of the intrinsic ATPase activity. In this paper, we report that EHD2 is specifically and stably associated with caveolae at the plasma membrane and not involved in clathrin-mediated endocytosis or endosomal recycling, as previously suggested. EHD2 interacts with pacsin2 and cavin1, and ordered membrane assembly of EHD2 is dependent on cavin1 and caveolar integrity. While the EHD of EHD2 is dispensable for targeting, we identified a loop in the nucleotide-binding domain that, together with ATP binding, is required for caveolar localization. EHD2 was not essential for the formation or shaping of caveolae, but high levels of EHD2 caused distortion and loss of endogenous caveolae. Assembly of EHD2 stabilized and constrained caveolae to the plasma membrane to control turnover, and depletion of EHD2, resulting in endocytic and more dynamic and short-lived caveolae. Thus, following the identification of caveolin and cavins, EHD2 constitutes a third structural component of caveolae involved in controlling the stability and turnover of this organelle.**

Monitoring Editor
Sandra Lemmon
University of Miami

Received: Sep 15, 2011
Revised: Jan 31, 2012
Accepted: Feb 2, 2012

INTRODUCTION

Internalization and recycling of cell surface receptors involves multiple membrane sculpting and budding events in the cell. Proteins within the Eps15 homology domain–containing protein family (EHDs) have been shown to participate in the remodeling of membranes in the endosomal system (reviewed in Naslavsky and Caplan, 2011). The mammalian genome encodes four EHDs, EHD1–4, while *Caenorhabditis elegans* and *Drosophila* each has a single EHD gene, *rme-1* and *Past-1*, respectively. EHDs contain an amino (N)-terminal GTPase (G) domain, followed by a helical domain, a linker region, and a C-terminal EHD known to bind to linear Asn-Pro-Phe peptide (NPF) motifs (Figure 1A). We previously solved the crystal structure of EHD2, revealing that EHDs are dynamin-related proteins involved in nucleotide-dependent membrane remodeling (Daumke *et al.*, 2007). EHD2 dimerizes via a conserved interface within the G domain and a highly curved membrane-binding site is created by the tips of the two opposing helical domains (Figure 1A). In addition to residues enforcing sterical hindrance, binding of the EHD to the top of the opposing G domain makes the G domain bind and hydrolyze ATP rather than GTP. We found that ATP hydrolysis was stimulated by liposome binding and oligomerization of EHD2 into ring-like structures on a membrane surface, causing remodeling of liposomes into highly curved membrane tubules (Daumke *et al.*, 2007).

This article was published online ahead of print in MBoC in Press (http://www.molbiolcell.org/cgi/doi/10.1091/mbc.E11-09-0787) on February 9, 2012.

The authors declare no competing interests.

Address correspondence to: Richard Lundmark (Richard.lundmark@medchem.umu.se).

Abbreviations used: BHK, baby hamster kidney; CTxB-HRP, cholera toxin B-subunit–horseradish peroxidase; DAB, diaminobenzidine; DTT, dithiothreitol; EHD2, Eps15 homology domain–containing 2; EMCCD, electron-multiplying charge-coupled device; FRAP, fluorescence recovery after photobleaching; G, GTPase domain; GFP, green fluorescent protein; GST, glutathione *S*-transferase; ICQ, intensity correlation quotient; immunoEM, immunoelectron microscopy; ITC, isothermal titration calorimetry; M6PR, mannose 6-phosphate receptor; MβCD, methyl β-cyclodextrin; MHC-1, major histocompatibility complex I; NA, numerical aperture; NPF, Asn-Pro-Phe peptide; PBS, phosphate-buffered saline; RFP, red fluorescent protein; siRNA, small interfering RNA; SNX9, sorting nexin 9; TfnR, transferrin receptor; TIRF, total internal reflection fluorescence.

© 2012 Morén *et al.* This article is distributed by The American Society for Cell Biology under license from the author(s). Two months after publication it is available to the public under an Attribution–Noncommercial–Share Alike 3.0 Unported Creative Commons License (http://creativecommons.org/licenses/by-nc-sa/3.0).

"ASCB®," "The American Society for Cell Biology®," and "Molecular Biology of the Cell®" are registered trademarks of The American Society of Cell Biology.

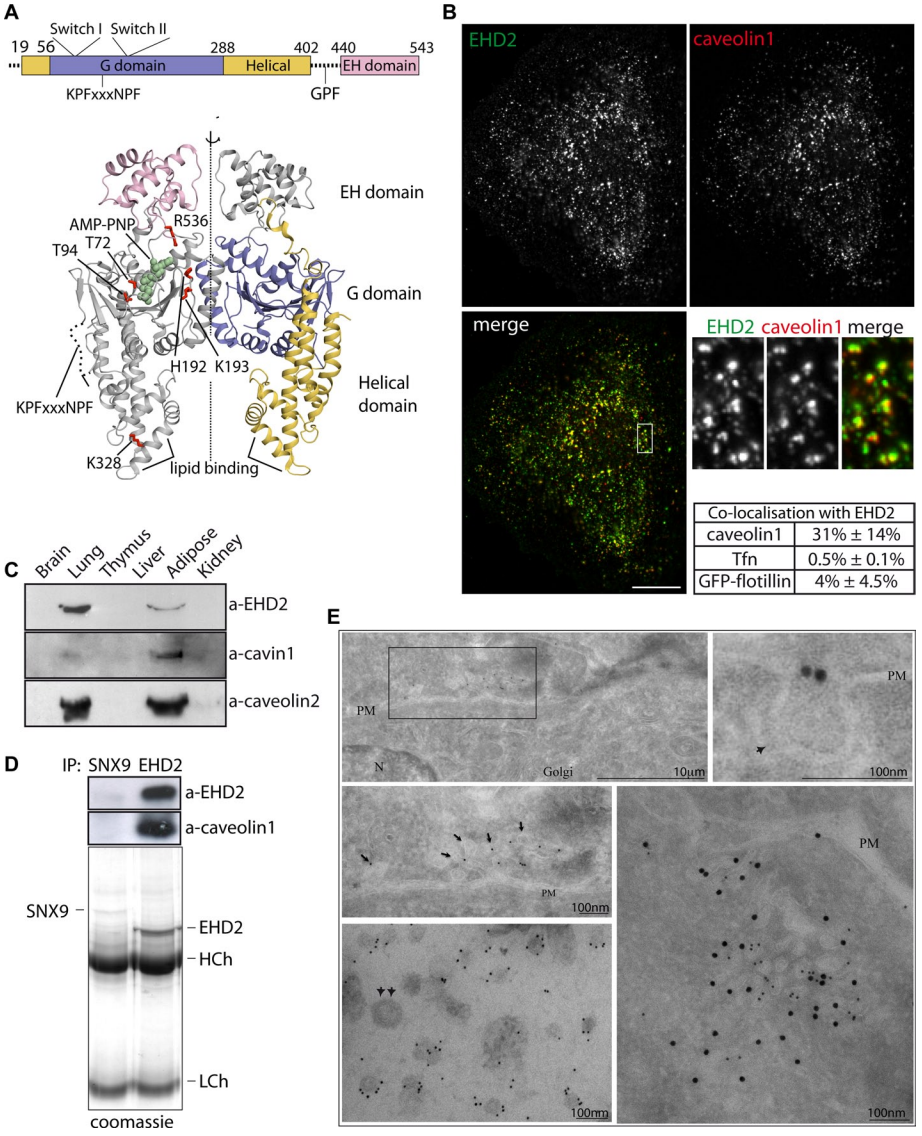

FIGURE 1: EHD2 localizes specifically to caveolin1-positive caveolae. (A) Schematic domain representation, with the positions of specific sequence motifs indicated. The three-dimensional structure of dimeric EHD2 (pdb 2QPT) is shown as a cartoon representation with key residues discussed in this study shown as red sticks and the nonhydrolyzable ATP analogue as green balls. (B) Fluorescence micrograph of HeLa cells stained for endogenous EHD2 and caveolin1. Scale bar: 10 µm. In the table, colocalization between EHD2 and indicated proteins is quantified from three individual merged images for each experiment (see also Figure S1, E and G, for representative images). (C) Equal protein amounts of different tissue lysates were analyzed by SDS–PAGE and immunoblotting using antibodies against EHD2, cavin1, and caveolin2. (D) Immunoprecipitations of EHD2 and SNX9 from a lysate of lung membranes were separated on SDS–PAGE, which was followed by Western blotting with the indicated antibodies. The bottom panel shows the Coomassie blue–stained gel. (E) Gallery of images showing immunoEM localization of endogenous EHD2 in 3T3-L1 cells. EHD2 associates with vesicular elements with the morphology of caveolae (arrows), including characteristic groups of caveolae at the cell surface. N, nucleus; PM, plasma membrane. The boxed area in the top panel is shown at higher magnification below. Top, right, magnification of EHD2-labeled caveolar structures. Bottom, right, double-labeling of EHD2 (10-nm gold) and cavin1-positive membranes (15-nm gold). Bottom, left, the immunoEM localization of EHD2 on plasma membrane lawns of 3T3-L1 adipocytes. EHD2 associates with vesicular profiles of 55- to 70-nm diameter characteristic of caveolae. Note the low labeling of flat plasma membrane and negligible labeling of clathrin-coated pits (double arrows).

In *C. elegans*, RME-1 was shown to be required for recycling of the yolk receptor (Grant *et al.*, 2001). A similar involvement in exit from the endosomal recycling compartment has been ascribed to EHD1 as part of the machinery for recycling of the transferrin receptor (TfnR) and major histocompatibility complex I (MHC-I; Lin *et al.*, 2001; Caplan *et al.*, 2002; Naslavsky *et al.*, 2004). Much less is known about the cellular roles of the other EHDs. Various reports have suggested that EHDs may form heterodimers (Galperin *et al.*, 2002; Lee *et al.*, 2005; Sharma *et al.*, 2008), and indeed both distinct and overlapping functions have been reported for the different EHDs (Naslavsky and Caplan, 2011). Sequence comparisons indicate EHD2 is the most distal member of the EHD family, and previous studies suggested an involvement in endocytosis of the insulin-responsive glucose transporter GLUT4 and the TfnR (Guilherme *et al.*, 2004). Interestingly, endogenous EHD2 was identified as being associated with caveolae in a mass spectrometry–based screen (Aboulaich *et al.*, 2004). Caveolae are characteristic small invaginations of the plasma membrane found abundantly in many cell types (reviewed in Bastiani and Parton, 2010). They are enriched in cholesterol, sphingolipids, and the proteins caveolin1–3 and cavin1–4 and have been implicated in various cellular processes as signaling domains, endocytic carriers, and sensors of membrane tension.

In this study, we aimed to further characterize the cellular function of EHD2. We found that EHD2 specifically bound and localized to caveolae to stabilize and control the dynamics of such invaginations at the cell surface. The ability of EHD2 to oligomerize and remodel and stabilize membrane surfaces was shown to be regulated by ATP binding and hydrolysis, which probably reflects a common mechanism for the targeting and action of EHD proteins.

RESULTS

Endogenous EHD2 specifically binds and localizes to caveolae

To identify the precise site of action and cellular role of EHD2, we generated affinity-purified antibodies against full-length EHD2 that specifically detected recombinant EHD2, but not EHD1, -3, and -4, in immunoblotting (see Supplemental Figure S1A). In HeLa cells, the antibodies specifically recognized overexpressed green fluorescent protein (GFP)-EHD2 in tubules and punctate structures (Figure S1B). No colocalization was seen in cells overexpressing GFP-tagged EHD1, but, as in untransfected cells, punctate structures were labeled. To validate that these structures represent endogenous EHD2, we used small interfering RNA (siRNA) to deplete EHD2 in HeLa cells, which indeed resulted in ablation of the distinct punctate labeling pattern (Figure S1, C and D). To elucidate the

nature of the punctate location of EHD2, we colabeled cells using the EHD2 antibody and antibodies against markers of various compartments. We found extensive colocalization between EHD2 and caveolin1-positive punctate structures, indicating that most of the membrane-associated EHD2 is found in caveolae (Figure 1B). In contrast, we found no colocalization with flotillin (quantified in Figures 1B and S1E), which generates specific subdomains in the membrane in a manner similar to caveolin1 (Glebov *et al.*, 2006). EHD2 has been suggested as functioning in both exit from endosomes and clathrin-dependent endocytosis (Guilherme *et al.*, 2004; George *et al.*, 2007). However, we found no colocalization with recycling MHC-I molecules or mannose-6-phosphate receptors (M6PR). Neither did we observe any colocalization with AP-2–coated structures or endocytosed transferrin (Figure S1, F and G). We also assayed markers for the endoplasmic reticulum, Golgi, and early and late endosomes without finding any significant colocalization (Figure S1G).

Consistent with a role of EHD2 at caveolae, EHD2 was highly expressed in tissues known to have abundant caveolae, such as lung and adipose tissue, in which caveolin and cavin1 are also highly expressed (Figure 1C). To test whether markers of caveolae can be pulled down together with EHD2, immunoprecipitations from a membrane pool of mouse lung enriched for caveolin1 were performed. Indeed, caveolin1 was coimmunoprecipitated with EHD2 from this lysate, showing that EHD2 interacts with caveolin1-positive membranes (Figure 1D). To prove that EHD2 is associated with caveolae on the surface, sections of cells were gold-immunolabeled with antibodies against EHD2 and cavin1 (Figure 1E). EHD2 associated with cavin-positive pits and vesicular profiles with the morphology of caveolae (Figure 1E, arrows), including characteristic groups of caveolae connected to the plasma membrane. This was confirmed using plasma membrane lawns labeled with antibodies against EHD2. This technique clearly demonstrated the presence of EHD2 on caveolae and the absence of EHD2 on flat plasma membrane and clathrin-coated pits (Figure 1E, bottom, left).

EHD2 is firmly and specifically associated with stable caveolae on the plasma membrane

Overexpressed EHD2 in HeLa cells localizes to both punctae and membrane tubules (Daumke *et al.*, 2007; Figure S1B). The tubular localization could be explained by the fact that HeLa cells have only low levels of caveolin1 and caveolae, leading to mislocalization and membrane tubulation by overexpressed EHD2. To determine whether caveolin1 expression drives EHD2 to caveolae, we analyzed the localization of overexpressed caveolin1–red fluorescent protein (RFP) and GFP-EHD2 in HeLa cells. When coexpressed, the two proteins showed striking colocalization in punctae, with almost all EHD2 found in caveolae but not in tubules (Figures 2A and S2A). GFP-tagged EHD1, -3, and -4 did not colocalize with caveolin1-RFP, showing that caveolar localization is a specific feature of EHD2 (Figure S3A). Interestingly, the expression of GFP- or myc-tagged EHD2, but not a membrane binding–deficient EHD2 mutant (EHD2 K328D), increased the localization of caveolin1-RFP, together with cavin1, on the cell surface (Figures 2A and S2, C and D). When expressed at high levels, caveolin1-RFP is known to accumulate in the endoplasmic reticulum and lysosomes and to aggregate due to improper sorting and assembly at the plasma membrane. Following ubiquitylation, unassembled caveolin1 is rapidly internalized for degradation (Hayer *et al.*, 2010b; Figure 2A). Our results indicate that membrane-bound EHD2 confines caveolin1 to the surface via recycling or retention at the plasma membrane.

To clarify whether EHD2 had a preference for association with internal or surface-associated caveolin1-positive structures, we determined the three-dimensional localization of caveolin1-RFP and GFP-EHD2 in living cells using confocal microscopy and image reconstructions. EHD2 was specifically found at the plasma membrane, at which it colocalized with the surface pool of caveolin1, although caveolin1-RFP was also detected in internal structures (Figure 2B). To confirm this observation, we used total internal reflection fluorescence (TIRF) microscopy combined with epifluorescence microscopy and followed the localization of caveolin1-RFP and GFP-EHD2 within the cell. Indeed, EHD2 was mainly detected at the cell surface, together with caveolin1 (Figure S3B). Although a subset of EHD2- and caveolin1-positive structures were endocytosed, the majority of such structures appeared limited in their lateral diffusion and stably associated with the cell surface over time (Figure 2C). To determine whether EHD2 molecules were in continuous exchange or firmly bound to caveolae, we used fluorescence recovery after photobleaching (FRAP) microscopy to deplete the fluorescence signal in individual caveolae and follow the recovery of EHD2 and caveolin1. As previously shown (Thomsen *et al.*, 2002), caveolin1 did not recover significantly from bleaching within 10 min. In contrast, although the recovery of EHD2 fluorescence was also limited, EHD2 recovered considerably faster than caveolin1 within this time frame (Supplemental Movie S1 and Figure 2D). This finding indicates that caveolae-bound EHD2 has a slow exchange rate and rather stably associates with caveolae under these conditions.

Ordered membrane assembly of EHD2 is dependent on cavin and intact caveolae

Our data suggested that the membrane structure of caveolae, or proteins exposed in this environment, are required for EHD2 recruitment. We therefore used methyl β-cyclodextrin (MβCD), which is known to diminish caveolae, by decreasing the cholesterol content in the membrane (Rothberg *et al.*, 1992). This treatment resulted in loss of both endogenous and overexpressed EHD2, cavin, and caveolin1 in punctate structures, showing that cholesterol and caveolar integrity is crucial for higher-order assemblies of EHD2 (Figures 3A and S4, A–C). Note that the monoclonal antibody against caveolin1 reacted poorly toward caveolin1 in mouse 3T3-L1 cells, precluding detection of endogenous EHD2 and caveolin1 in the same cell. Shorter treatments with MβCD sometimes shifted the localization of endogenous and overexpressed EHD2 to larger tubular structures totally separated from caveolin1-positive structures (Figures 3B and S4D). This indicates that EHD2 can temporally bind and remodel membranes in the absence of intact caveolae, similar to EHD2 expression in cells without caveolae. Biochemical determination of the amount of membrane-bound and cytosolic EHD2 showed that similar amounts of EHD2 were bound to the membrane in control and MβCD-treated cells (Figure S4E). This indicates that ordered EHD2 assembly, but not EHD2 membrane binding per se, is dependent on cholesterol, in agreement with previous liposome-binding experiments using purified EHD2 (Daumke *et al.*, 2007). Following depletion of cholesterol, or other perturbations of caveolar assembly, caveolin1 was recently shown to disperse and become endocytosed into endosomes and degraded (Hill *et al.*, 2008; Hayer *et al.*, 2010b); however, our data suggest that EHD2 is not involved in this uptake due to the lack of colocalization with internalized caveolin1 following MβCD treatment.

EHD2 interacts and colocalizes with cavins and pacsin2

The special lipid composition and presence of structural integral membrane proteins, such as caveolin, render caveolae difficult to

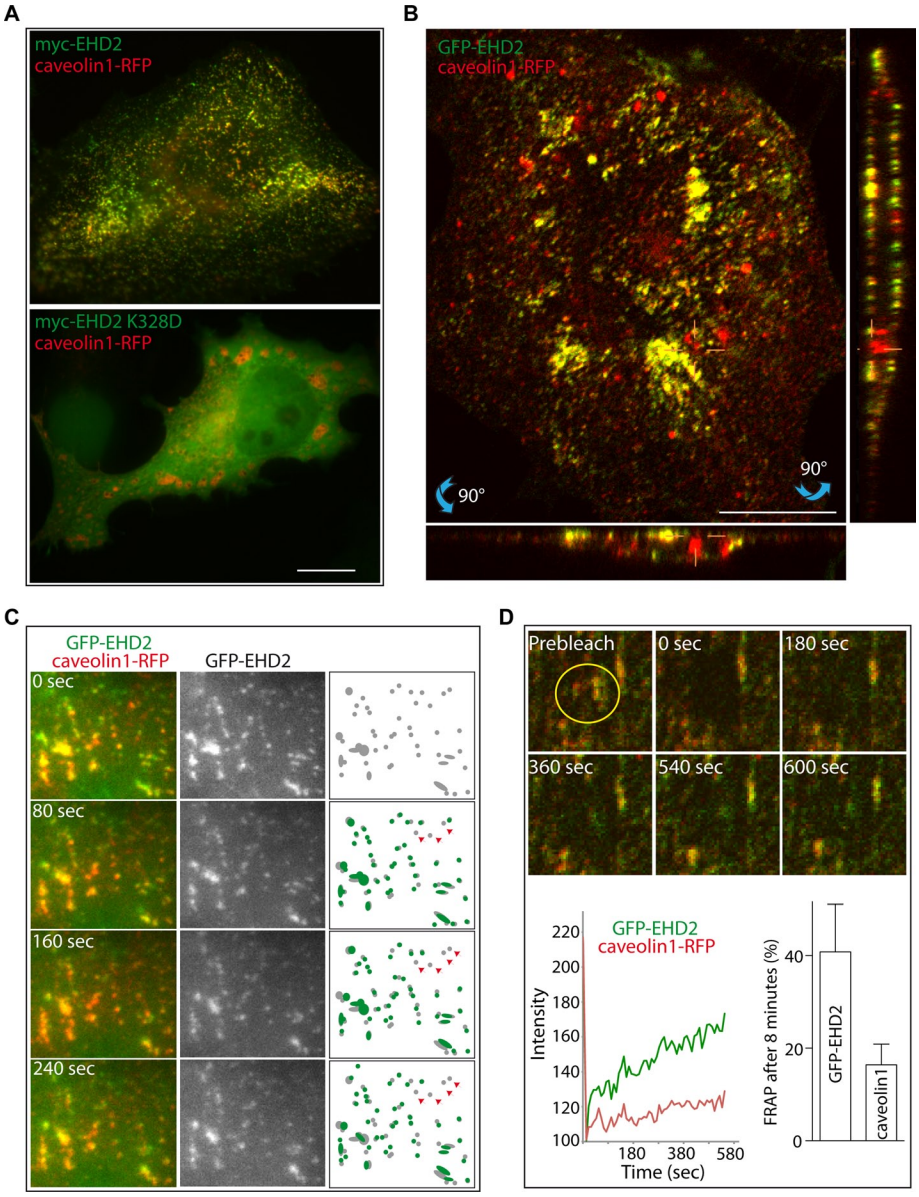

FIGURE 2: EHD2 is stably associated with steady caveolae on the plasma membrane. (A) Epifluorescence micrographs of HeLa cells expressing caveolin1-RFP together with myc-EHD2 (top) or the membrane binding–deficient mutant myc-EHD2 K328D (bottom). (B) Confocal sections of living 3T3-L1 cell transfected with GFP-tagged EHD2 and RFP-tagged caveolin1. Bottom and side projections show slices of the merged maximum projections at position indicated by yellow cross-hairs at 90° rotation. Note the colocalization at the cell surface. (C) Representative fluorescence micrographs of 3T3-L1 cells transfected with GFP-EHD2 and caveolin1-RFP and analyzed by TIRF microscopy for 4 min with images taken every second. Structures positive for EHD2 and caveolin1 were schematically tracked at the indicated time points (green circles) and overlaid on the schematic illustration of structures at time zero (gray circles). Disappearing structures symptomatic of endocytosis are indicated by red arrowheads. (D) FRAP microscopy of 3T3-L1 cell transfected with GPF-EHD2 and caveolin1-RFP. Distinct caveolae enriched in both proteins were bleached (yellow circle) and the time-dependent recovery of the fluorescence signal in this area was traced as indicated in the diagram below. Bar graph showing FRAP of GFP-EHD2 and caveolin1-RFP after 8 min as quantified from three independently bleached regions. Error bars represent SD. All scale bars: 10 μm.

membrane; this was followed by immunoprecipitation of EHD2 and sorting nexin 9 (SNX9, a control protein that associates with clathrin-coated pits). Cavin1 was immunoprecipitated together with EHD2 but not together with SNX9 (Figure 3C). In agreement with this, we found that recombinant EHD2 coupled to beads could specifically pull down cavin1 from a lung lysate (Figure 3D). In addition, we identified pacsin2 as an EHD2-associated protein. Pacsin2 was recently found to remodel caveolar membranes and influence the shape of caveolae (Hansen *et al.*, 2011; Senju *et al.*, 2011). Using the EHD of EHD2 as bait, we confirmed that this domain is responsible for binding to pacsin2, which in pull-downs from lung lysates is the major interaction partner of the EHD (Figure 3E). Using isothermal titration calorimetry (ITC), we found that one EHD2 dimer binds to one pacsin2 molecule with an affinity of 37 μM (Figures 3F and S5, A–D). This interaction did not depend on the SH3 domain of pacsin2 but on the integrity of the three NPF motifs, which is in agreement with previous studies showing that EHDs of EHD proteins interact with the NPF motifs of pacsins (Braun *et al.*, 2005). Furthermore, two isolated EHDs also bound to one pacsin2 molecule with somewhat lower affinity, indicating that dimerization of EHD2 can increase the avidity for its substrate.

Pacsin2 and all four members of the cavin protein family (cavin1–4) localize to caveolae and have partially overlapping functions (Hill *et al.*, 2008; Bastiani *et al.*, 2009; Hansen *et al.*, 2009; McMahon *et al.*, 2009; Senju *et al.*, 2011). To test whether EHD2 localizes to caveolae together with pacsin2 and the cavins, we coexpressed EHD2 together with individual cavins and stained for pacsin2 or caveolin1 (Figures 3G and S5E). We found a robust colocalization of EHD2 with all four cavins on caveolae. Interestingly, we observed that pacsin2 only colocalized with a subset of EHD2- and caveolin1-positive structures, but, in addition, decorated structures devoid of both EHD2 and caveolin1 (Figure 3G). Taken together, these results suggest a tight interplay of EHD2, cavins, and pacsin2 at caveolae. However, while EHD2 and cavins can be considered as general components, pacsin2 appears to be only temporary recruited or localized to a specific subset of caveolae.

analyze with traditional biochemical approaches. However, EHD2 and cavin1 are peripheral membrane proteins, which allowed us to determine whether these proteins interacted using immunoprecipitation. We prepared membranes from mouse lung and dissolved them in 0.5% NP40 and high salt to wash EHD2 off the caveolar

The KPF loop, but not the EHD, is required for caveolar targeting

Oligomerization of EHD2 as a result of membrane binding and interactions between the G domains of EHD2 dimers (Figure 4A) was proposed to activate ATP hydrolysis (Daumke *et al.*, 2007). The

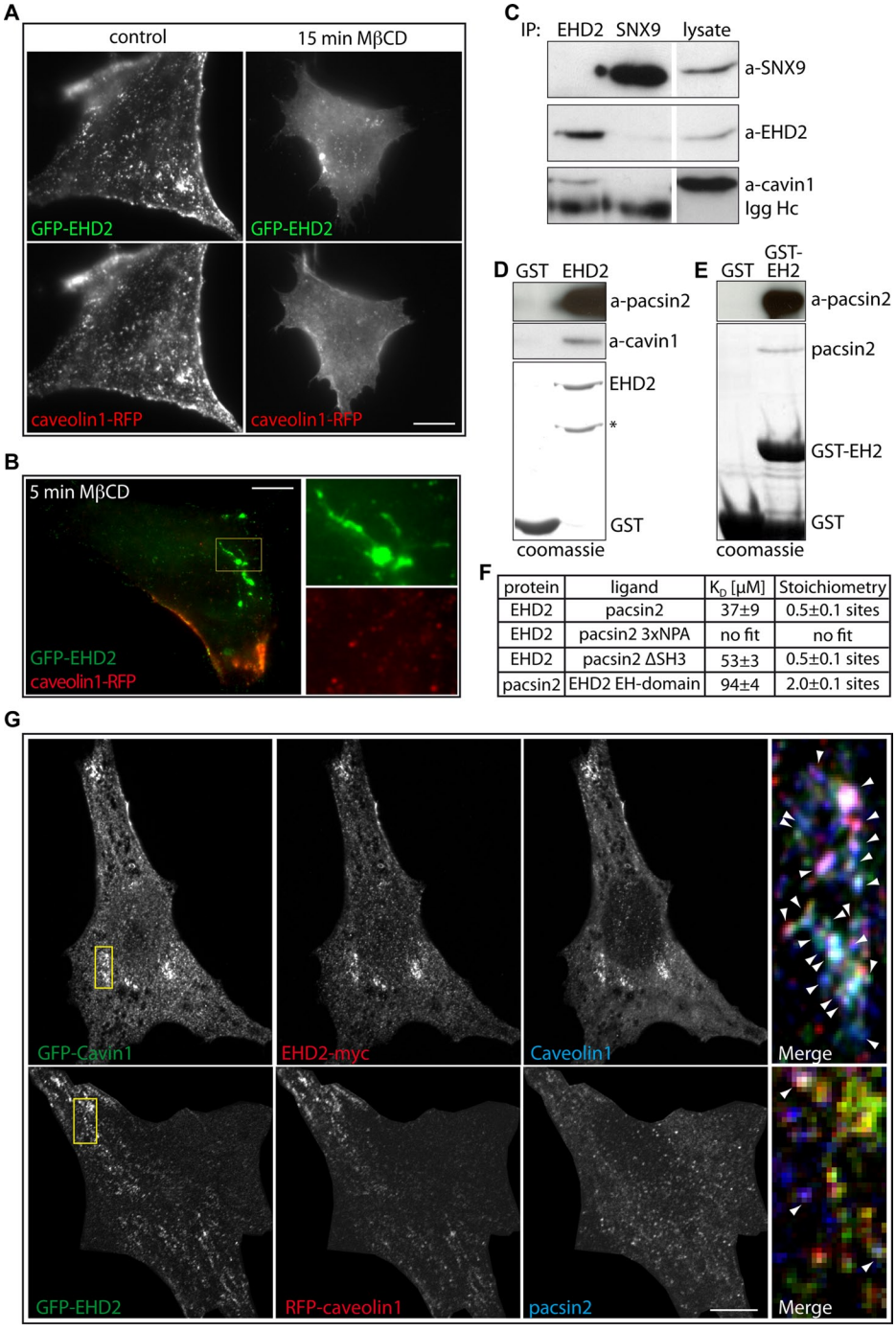

FIGURE 3: EHD2 interacts and colocalizes with pacsin2 and cavin1, and caveolar membrane integrity is required for ordered membrane assembly of EHD2. (A and B) Fluorescence micrographs of 3T3-L1 cells coexpressing GFP-EHD2 and caveolin1-RFP and treated with 15 mM MβCD for 5 or 15 min or PBS (control). Insets in (B) show magnifications of the boxed area. (C) Immunoprecipitates of EHD2 and SNX9 from mouse lung lysates were analyzed by SDS–PAGE and immunoblotting with antibodies against the indicated proteins. (D and E) Pull-down experiments from lung lysate using purified GST, EHD2, or GST-tagged EHD of EHD2 coupled to Sepharose beads were analyzed by SDS–PAGE Coomassie blue staining and immunoblotting with antibodies against cavin1 and pacsin2. * indicates degraded EHD2 protein. (F) Table showing the dissociation constants and stoichiometry for the interaction of EHD2 with pacsin2 obtained by ITC. See also Figure S5. (G) Fluorescence micrographs of 3T3-L1 cells coexpressing myc-EHD2 and GFP-cavin1 and costained for endogenous caveolin1 (top panel), or GFP-EHD2 and caveolin1-RFP and costained for endogenous pacsin2 (bottom panel). Insets show merged image magnifications of areas indicated by yellow rectangles. White arrowheads indicate structures positive for all three proteins. All scale bars: 10 μm.

EHDs were shown to localize to the "top binding site" of the opposing G domain, at which they also bind to a GPF motif in the linker region between the helical domain and EHD. At that position, the EHDs sterically block oligomerization of the G domains. It was suggested that switching of the EHDs to a KPFxxxNPF motif (residues 120–128) in a disordered loop at the side of the G domain releases autoinhibition and promotes oligomerization. (Daumke *et al.*, 2007; Figure 4A). To assay whether transition of the EHD to the KPFxxxNPF motif is indeed required for caveolar localization, we expressed a mutant in the motifs (EHD2 F122A/F128A) that was previously shown to lack membrane-stimulated ATPase activity (Daumke *et al.*, 2007). Surprisingly, this mutant was unable to localize to caveolae and did not affect the localization of endogenous caveolin1 (Figure S6A). We further assayed the F122A and F128A mutations individually, as well as mutations in nearby amino acids in the unstructured loop. The F128A mutant behaved in a manner similar to wild-type EHD2, whereas the F122A and K120N mutants were found in punctate and tubular structures distinct from caveolin1-positive structures (Figures 4B and S6B). We conclude that the KPF motif is required for caveolar targeting.

In one possible scenario, binding of the EHD to the KPF loop relieves an autoinhibitory interaction and/or promotes stable oligomerization of the adjacent G domains. Alternatively, the KPF loop is directly involved in caveolar targeting by binding to another caveola-specific protein. To distinguish between these possibilities, we generated EH deletion mutants in the context of wild-type EHD2 (EHD2 $\Delta EH_{1–416}$) or the F122A mutant (EHD2 F122A/$\Delta EH_{1–416}$). Strikingly, the ΔEH mutant localized to caveolae in a manner similar to wild-type EHD2 indicating that, in contrast with other EHDs (Caplan *et al.*, 2002; Galperin *et al.*, 2002; George *et al.*, 2007; Sharma *et al.*, 2008), the EHD of EHD2 is not required for proper targeting. Interestingly, EHD2 F122A/ΔEH did not colocalize with caveolin1 (Figure 4, C and D), indicating that it is not the release of an autoinhibitory action of the EHD from the top site that is responsible for the missing membrane targeting of the F122A mutant. To determine whether the KPF loop is directly involved in caveolar targeting, we assayed whether recombinant EHD2 and EHD2 F122A attached to beads could bind to caveolae from detergent-solubilized membranes. EHD2, but not glutathione *S*-transferase (GST), bound to caveolae, and

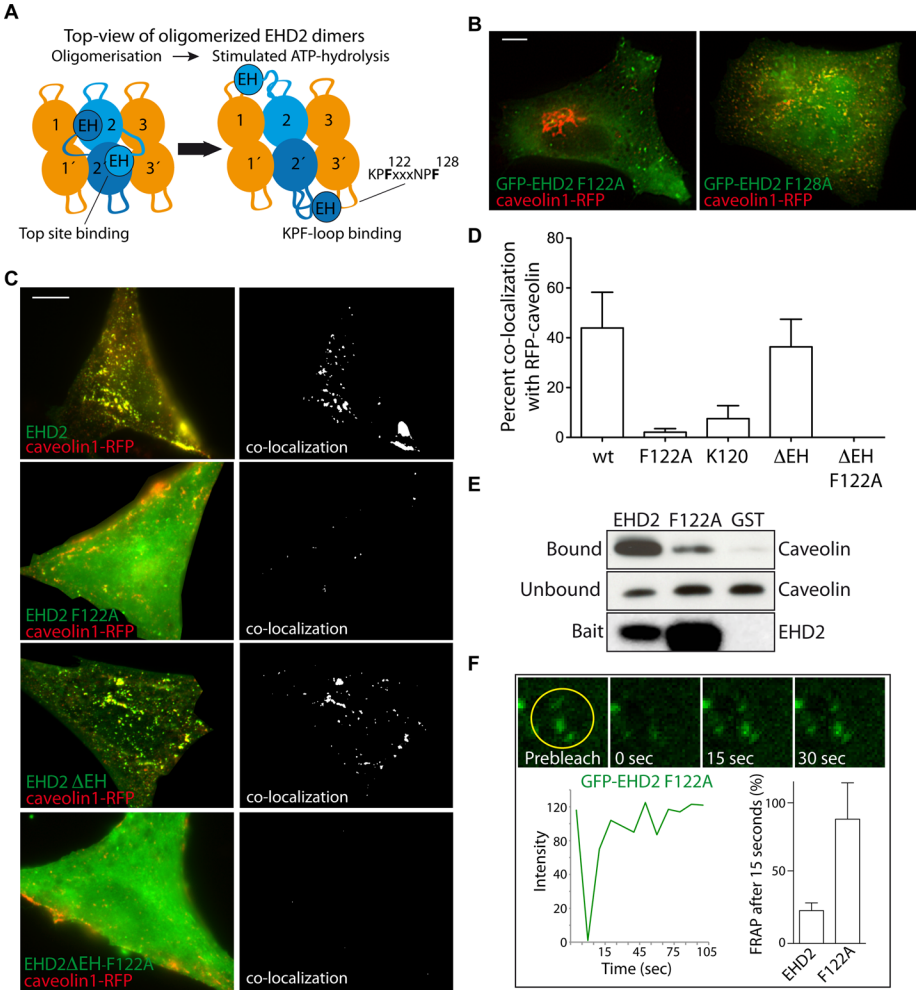

FIGURE 4: The KPF loop in EHD2 mediates targeting to caveolae and stable membrane assembly of EHD2. (A) Schematic illustration of the previously proposed oligomerization model of EHD2 and subsequent stimulation of ATP hydrolysis. Top views of three EHD2 dimers shows the proposed transition of the EHDs from the top site of the GTPase domain to the KPF loop of the GTPase domain. (B and C) Fluorescence micrographs of 3T3-L1 cells coexpressing GFP-tagged EHD2 variants and caveolin1-RFP. The ΔEH mutant comprises residues 1–416. (C) Colocalizing pixels are shown on the right panels. (D) Bar graph showing quantification of the extent of colocalization between GFP-tagged EHD2 variants and caveolin1-RFP using three individual merged images for each construct. Error bars represent SD. (E) Pull-down experiments from caveolae-enriched membranes using purified GST, EHD2, or EHD2-F122A coupled to Sepharose beads were analyzed by SDS–PAGE and immunoblotting with antibodies against caveolin1 and EHD2. (F) FRAP microscopy of 3T3-L1 cell transfected with GPF-EHD2 F122A and caveolin1-RFP. The indicated area (yellow circle) was bleached and the time-dependent recovery of the fluorescence signal in this area was traced as shown in the diagram below. Bar graph showing FRAP of GFP-EHD2 and GFP-EHD2 F122A after 15 s as quantified from three independently bleached regions for each protein. Error bars represent SD. All scale bars: 10 μm.

the F122A mutant was drastically impaired in caveolar binding, indicating that the KPF motif, but not oligomerization, is directly required for caveolar binding (Figure 4E). We next assayed the stability of the EHD2 F122A assemblies devoid of caveolin using FRAP microscopy. Membrane assembly of this mutant in tubules and punctae was found to be strikingly dynamic in comparison with wild-type EHD2, with almost complete recovery after 15 s (Supplemental Movie S2 and Figure 4F). Taken together, our data suggest that loop-mediated targeting and further assembly of EHD2 leads to stable association with caveolae. Without this specificity, EHD2 demonstrates dynamic membrane binding and membrane remodeling.

Nucleotide binding is required for caveolar localization of EHD2, and ATP hydrolysis promotes remodeling of caveolae

The ATP-dependent membrane-remodeling activity of EHD2 suggested that EHD2 could be involved in the dynamics and turnover of caveolae. To clarify the role of ATP binding for caveolar targeting, we overexpressed an EHD2 mutant of the phosphate-binding loop (EHD2 T72A), which is unable to bind nucleotides (Daumke *et al.*, 2007). Indeed, this mutant was incapable of binding membranes and localizing to caveolae (Figure 5, A and B). This is in agreement with previous work in which we showed that oligomerization of EHD2 and subsequent membrane remodeling requires nucleotide binding in vivo and under stringent in vitro conditions (Daumke *et al.*, 2007). To address the role of ATP hydrolysis for the function of EHD2 at caveolae, we assayed the effect on caveolin1 following expression of EHD2 or EHD2 mutants with no or decreased ATPase activity (EHD2 T94A, EHD2 H192D, and EHD2 K193D) or EHD2 F122A (Daumke *et al.*, 2007). Interestingly, using immunoblotting, we found that endogenous caveolin1 was significantly down-regulated in EHD2-overexpressing cells (Figures 5, C and D, and 7C). EHD2, however, localized specifically to the remaining caveolin1-positive structures, and showed colocalization comparable with that of caveolin1-RFP (Figures 5, A and B). The level of endogenous EHD2 or cavin1 was not notably altered by the overexpression of GFP-tagged EHD2 variants (Figure 5C). Expression of EHD2 T94A also lowered the amount of endogenous caveolin1 to 58% of control cells and, in addition, affected the localization of both endogenous and overexpressed caveolin1, with fewer and larger aggregated structures or tubules (Figure 5A). Expression of other mutants with decreased ATPase activity (EHD2 K193D and EHD2 H192D) also showed this distortion of caveolae (Figure S7A). This indicates that in the absence of stimulated ATPase activity, caveolar morphology is disturbed by an increased membrane-remodeling activity of EHD2. Indeed, we observed that caveolin1-positive membranes were heavily tubulated by EHD2 T94A protein in some cells (Figure 5E). To investigate the effect of EHD2 overexpression at the ultrastructural level, baby hamster kidney (BHK) cells, which enable high transfection efficiency, were transfected with GFP-EHD2, GFP-EHD2 T94A, or GFP as a control. All constructs were expressed in more than 80% of cells, as judged by light microscopy. The cell surface was labeled with ruthenium red to allow the identification of surface-connected structures in thin sections. Caveolae were readily identified in control BHK cells as single pits or characteristic rosettes (Figure 6A). Expression of GFP-EHD2 and GFP-EHD2 T94A caused a consistent

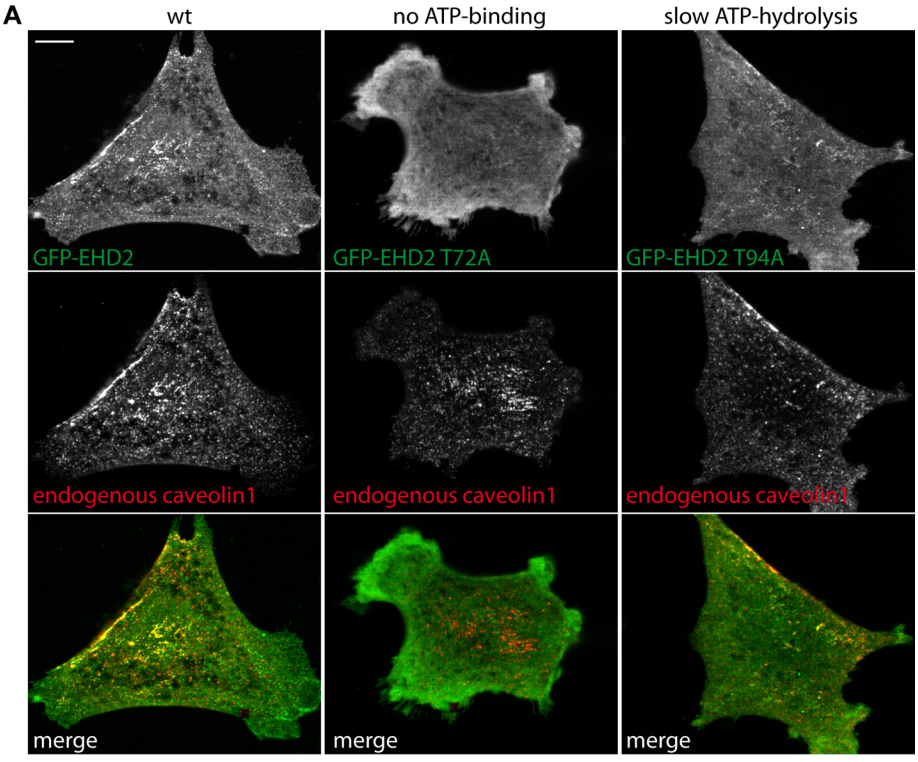

B

Percent localisation			ICQ values
EHD2	endo-caveolin	caveolin-RFP	caveolin-RFP
wt	43.9 ±4.8	30.6 ±2.1	0.374
T72A	1.7 ±0.6	0.2 ±0.1	0.084
T94A	30.5 ±6.7	11.1 ±4.2	0.163
H192D	30.3 ±4.7	ND	ND
K193D	10.8 ±1.8	ND	ND

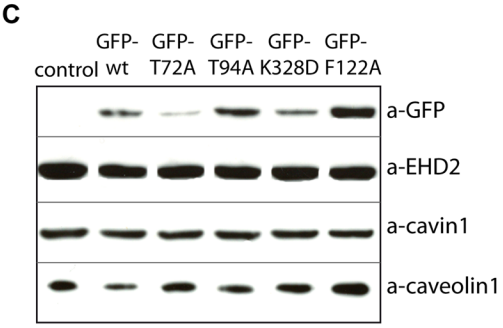

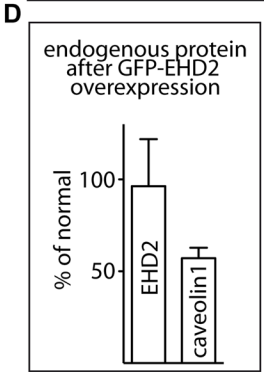

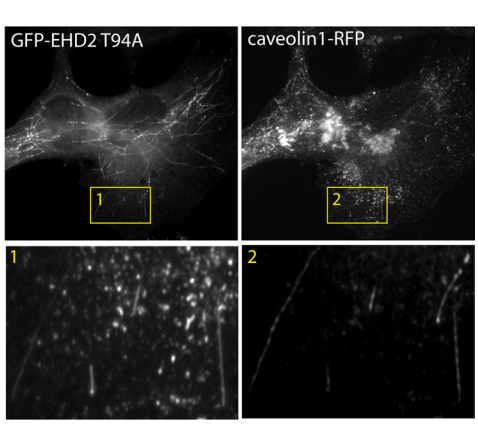

FIGURE 5: ATP-binding is required for EHD2 targeting, and ATP hydrolysis regulates the membrane-remodeling activity of EHD2. (A) Fluorescence micrographs of 3T3-L1 cells expressing GFP-tagged EHD2 variants and costained for endogenous caveolin1. (B) Quantification of the extent of colocalization between GFP-tagged EHD2 variants and endogenous caveolin1 or caveolin1-RFP. Three individual merged images from each experiment were normalized and the percentage of EHD2 structures that colocalized with caveolin1 or caveolin1-RFP were determined. ICQ values representing the extent of correlation in staining intensity (–0.5 [minimum] to 0.5 [maximum]) between GFP-tagged EHD2 variants and caveolin1-RFP were determined as described in *Materials and Methods*. (C) Immunoblot analysis of total protein levels in 3T3-L1 cells following overexpression of indicated GFP-tagged EHD2 variants. (D) Quantification of the levels of endogenous EHD2 and caveolin1 from three independent experiments as in (C). Error bars indicate the SD. (E) Fluorescence micrograph of cells coexpressing the ATP hydrolysis–deficient mutant GFP-EHD2 T94A and caveolin1-RFP showing heavily tubulated caveolin1-positive membranes colabeled with GFP-EHD2 T94. Insets show magnifications of indicated areas. All scale bars: 10 μm.

decrease in the density of surface caveolae (Figures 6, A and B). The remaining caveolae in the majority of cells showed normal morphology. However, highly expressing GFP-EHD2 cells showed striking accumulations of tubules, some of which were ruthenium red–labeled and therefore surface-connected (Figure 6A, black arrows), while others were of similar morphology but apparently disconnected from the cell surface (Figure 6A, white arrows).

Caveolae still form in cells depleted of EHD2

Loss of cavin1 has been shown to result in ablation of caveolae. To assay whether loss of EHD2 affected caveolae in 3T3-L1 cells, we used siRNA to deplete the levels of EHD2 and cavin1 (Figure 7A). We verified that we had at least 98% knockdown efficiency of EHD2 using siRNA by immunoprecipitating EHD2 from cells before immunoblotting (Figure 7A). When siRNA-treated cells were assayed by immunofluorescence, we found that the characteristic EHD2 stain was completely ablated (Figure 7B). Strikingly, caveolin1 localization and intensity appeared similar to that of cells treated with control siRNA. To verify that caveolin1 and cavin1 still localized to detergent-resistant caveolar membranes, we used siRNA to deplete EHD2 or cavin1, lysed the cells in 1% ice-cold Triton-100, and separated the membrane microdomains from dissolved membranes and cytosol by centrifugation. The pellet fraction (membrane microdomains) and supernatant were analyzed by immunoblotting to detect EHD2, cavin1, and caveolin1. As expected, depletion of cavin1 drastically reduced the amount of both caveolin1 and EHD2 in the pellet fraction due to the loss of caveolae (Figure 7, C and D). The total amount of caveolin1 was reduced, as previously shown (Hill *et al.*, 2008). However, when EHD2 was depleted, we detected a slight increase (32%) in caveolin1 levels. (Figure 7C). These data suggest that caveolae can still form in the absence of EHD2 or that the already formed caveolae were stable. To assay whether cells depleted of EHD2 were able to form new caveolae,

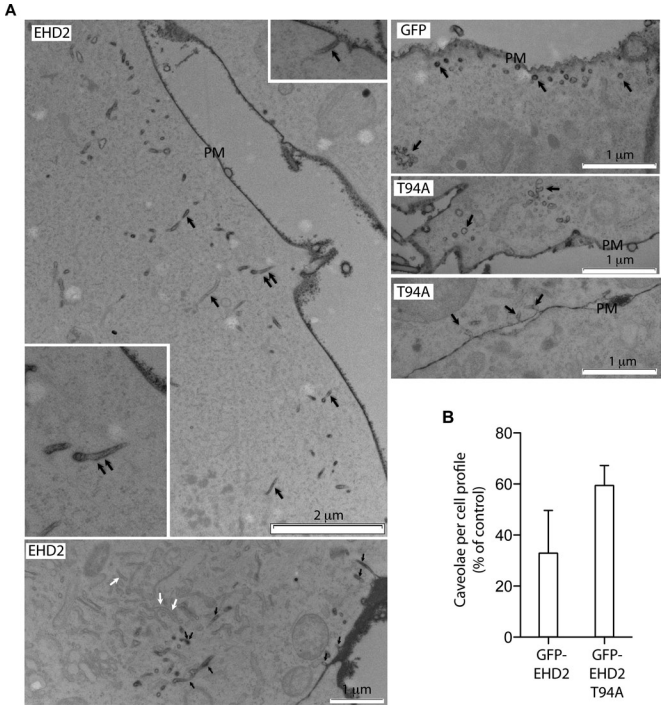

FIGURE 6: Ultrastructural characterization showing loss of surface-connected caveolae following overexpression of EHD2. (A) BHK cells were transfected with the indicated constructs, surface-labeled with ruthenium red, and then processed for Epon embedding. Caveolae were defined as ruthenium red–labeled, uncoated, circular profiles of 55- to 75-nm diameter. High expression of GFP-EHD2 causes formation of surface-connected tubules of ~45-nm diameter (arrows). In addition, tubules within the cytoplasm that are not surface connected are also evident (white arrows). Some tubules appeared coated (double arrows). Cells expressing the GFP-EHD2 T94A mutant (T94A) showed a range of morphologies, including caveolae similar to GFP control cells, small tubular caveolae, and in highly expressing aggregate-containing cells, loss of caveolae. PM, plasma membrane. (B) Bar graph showing the quantification of the number of surface-connected caveolae per cell profile in GFP-EHD2– or GFP-EHD2 T94A–expressing cells compared with GFP control cells as the mean of three independent quantifications. Error bars represent SEM. Highly expressing GFP-EHD2 cells, containing prominent aggregates, were excluded.

we removed caveolae by MβCD treatment and analyzed the recovery of caveolae after washing away the drug. In control cells, as well as in EHD2-depleted cells, caveolae started to reappear after 30 min and had fully recovered after 2 h (Figure 7E). Taken together, these data showed that caveolae are present in cells lacking EHD2 and that caveolar structures can re-form in the absence of EHD2 after restoration of cholesterol levels.

Caveolae are more dynamic in cells lacking EHD2

Caveolae have been described as relatively stable structures with the ability to undergo stimulated fission and endocytosis (Thomsen *et al.*, 2002; Hommelgaard *et al.*, 2005). However, in stable caveolin1-GFP–expressing cells, a pool of caveolae was observed to be much more dynamic and to display a kiss-and-run behavior (Pelkmans and Zerial, 2005; Boucrot *et al.*, 2011). To assay whether EHD2 was involved in regulating the dynamics of caveolae, we first used an ultrastructural assay (Kirkham, 2005; Howes, 2010; Boucrot *et al.*, 2011) to quantify the number of budded caveolae. This assay relies on internalization of cholera toxin B-subunit–horseradish peroxidase (CTxB-HRP) for 1 min and then quantification of budded caveolae (defined as 55- to 75-nm uncoated profiles) via the diaminobenzidine (DAB) reaction in the presence of a surface-quenching agent (Kirkham, 2005). Interestingly, in comparison with control cells, EDH2-depleted cells displayed 2.5 times more internalized caveolae at this time point (Figure 8, A and B). Using dynasore treatment to block dynamin resulted in greatly reduced caveolar endocytosis, as previously described (Figure 8B; Boucrot *et al.*, 2011). We observed that the total number of surface-connected caveolae was slightly increased in cells lacking EHD2, in contrast with cells overexpressing EHD2 (Figure 8C). These data suggest that the more dynamic endocytic caveolae might fuse back to the plasma membrane more efficiently in the absence of EHD2, resulting in more caveolae at the surface. We detected no obvious morphological phenotypic changes in caveolae following EHD2 depletion (unpublished data). To address whether EHD2 stabilized caveolae at the plasma membrane, we used TIRF microscopy to look at the dynamics of surface-associated caveolin1-RFP following expression of GFP-EHD2 or GFP-EHD2 K328D. Strikingly, cavolin1-RFP was highly dynamic on the surface when expressed together with the membrane binding–deficient GFP-EHD2 K328D, which likely functions to sequester endogenous EHD2 (Supplemental Movie S3, A and B, and Figure 8D, bottom). However, in cells expressing GFP-EHD2, caveolin1-RFP was found together with EHD2 in structures that were very stable and did not show any apparent membrane diffusion (Supplemental Movie S4, A and B, and Figure 8D, top). These results indicate that EHD2 is needed to stabilize caveolae at the surface and suggested that such structures are spatially constrained, possibly through coupling to the cytoskeleton. On the basis of our results, we propose a model in which ATP binding and the KPF loop target EHD2 to caveolae, and subsequent oligomerization of EHD2 sculpts the caveolar membrane to stabilize caveolae at the cell surface and control scission from the membrane (Figure 8E).

DISCUSSION

EHDs are widely used in trafficking processes throughout the cell, but little is known about their detailed cellular function and the determinants that mediate specificity in their recruitment to particular trafficking pathways. In this paper, we show that EHD2, but not other EHDs, is specifically associated with caveolae at the cell surface. Ordered membrane assembly of EHD2 was dependent on ATP binding and caveolar integrity. Interestingly, the unstructured KPF loop at the periphery of the G domain is directly involved in targeting of EHD2 dimers to caveolae. Recruitment could be mediated via proteins exposed on the surface of caveolae and influenced by the specific lipid composition and membrane curvature of caveolae. Immobilized EHD2 was able to pull down caveolae in vitro, demonstrating that EHD2 dimers are sufficient for caveolar binding. Due to the biochemical properties of caveolin1, analysis of direct interactions with EHD2 was precluded. However, EHD2 was found to interact with cavin1 and pacsin2, suggesting a direct association with core components of caveolae. Binding to pacsin2 was mediated via the EHD, but targeting of EHD2 to caveolae was independent of the EHD, indicating that pacsin2 is not responsible for recruiting EHD2. In contrast to other EHDs (Kieken *et al.*, 2010), the EHDs might rather be involved in the intramolecular control of EHD2 activity and, possibly, subsequent protein interactions at caveolae. Consistent with these findings, Hansen *et al.* recently reported that GFP-EHD2 localized to morphologically defined caveolae as seen by immunoelectron microscopy (immunoEM; Hansen *et al.*, 2011).

At the plasma membrane, caveolin1-enriched domains adopt the typical invaginated structure of caveolae in a cholesterol-, caveolin1-,

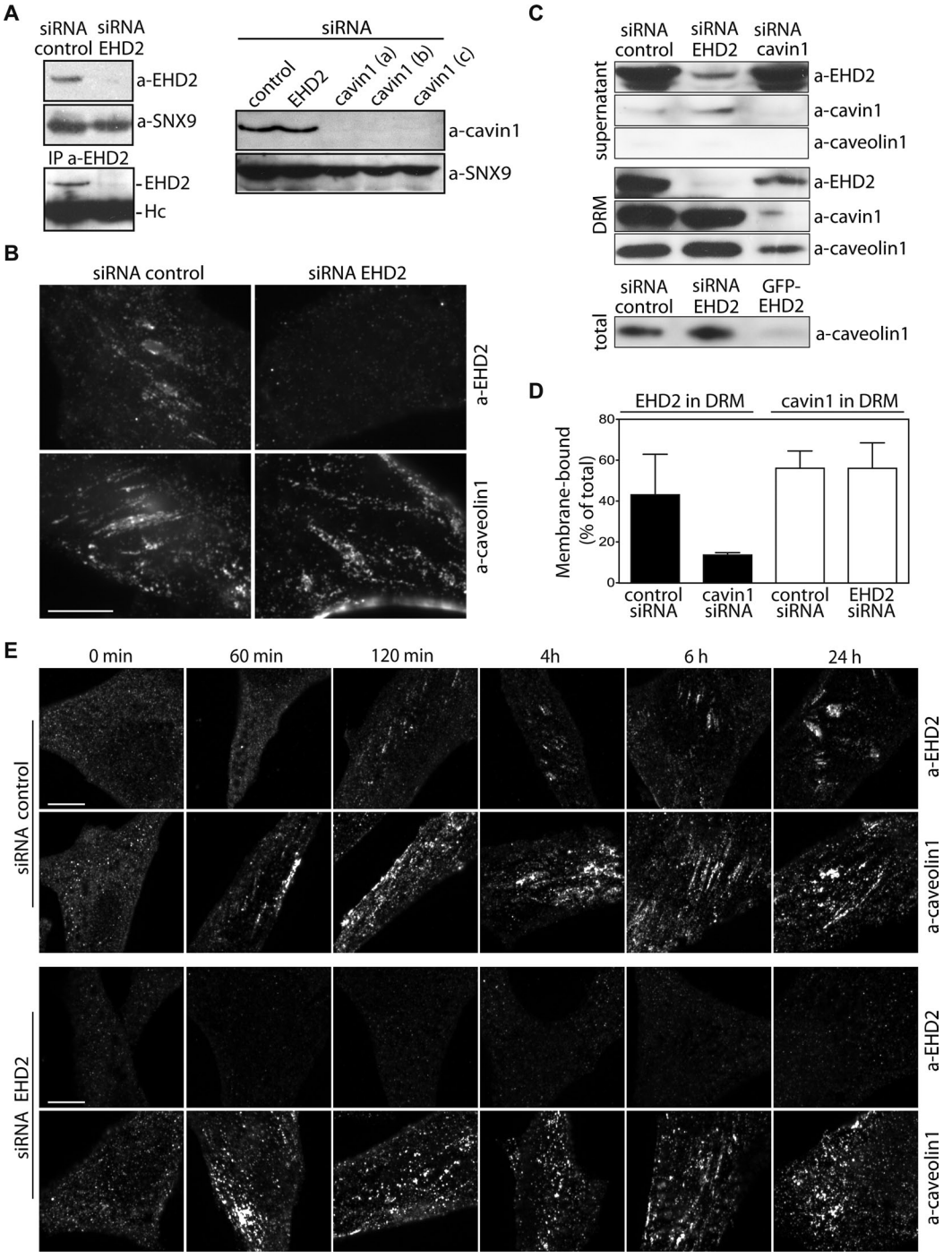

FIGURE 7: EHD2 is not required for the formation of caveolae. (A) 3T3-L1 cells were treated with siRNA against EHD2 or three different cavin1 siRNAs or control siRNA. Cell lysates (top, left and bottom panels) or immunoprecipitates (top, right) obtained using EHD2 antibodies antibodies (top, right panel) were subjected to SDS–PAGE and analyzed by immunoblotting with the indicated antibodies. (B) Fluorescence micrographs of cells treated with siRNA against EHD2 or control siRNA and stained for EHD2 or caveolin1. Note that the monoclonal antibody against caveolin1 reacted poorly toward caveolin1 in mouse 3T3-L1 cells, so we were not able to detect endogenous EHD2 and caveolin1 in the same cell. (C) Cells treated as in (A), or overexpressing GFP-EHD2, were lysed and either boiled directly in sample buffer (total) or detergent-resistant membranes (DRM) were separated from cytosol and soluble membranes (supernatant) by centrifugation. Fractions were analyzed by immunoblotting using the indicated antibodies. The total level of caveolin1 in EHD2-depleted cells was 132 ± 18% compared with control cells, as determined from three independent experiments. Error values represent SEM. (D) Bar graph showing quantification of the EHD2 and cavin1 fraction in detergent-resistant membranes in control cells and cells depleted of EHD2 or cavin1. Immunoblots of EHD2 and cavin1 from three individual experiments as in (C) were quantified and scored as percentage of total protein. Error bars show SD. (E) Control cells and cells depleted of EHD2 were treated with 10 mM MβCD for 20 min to deplete caveolae. MβCD was washed out, and cells were fixed and stained for EHD2 or caveolin1 at the indicated time points. Note that caveolin1 staining recovered similarly in the absence and presence of EHD2. All scale bars: 10 μm.

and cavin-dependent manner (Bastiani and Parton, 2010). While caveolin1 might induce membrane curvature of caveolae via oligomerization and its stable integration in the membrane (Parton and Simons, 2007; Hayer *et al.*, 2010a), cavin1–4 form peripherally associated multiprotein complexes that regulate the morphology and dynamics of caveolae (Hill *et al.*, 2008; Bastiani *et al.*, 2009; Hansen *et al.*, 2009; McMahon *et al.*, 2009). Together with pacsin2, EHD2 is the first-described caveola-associated peripheral protein with biochemically defined, membrane-remodeling activity. Interestingly, EHD2 oligomers in vitro were found to adopt rings of varying diameter that closely matched the distinct size of caveolae (Daumke *et al.*, 2007). We show that caveolar membranes are remodeled into long tubules in the complete absence of ATP hydrolysis in EHD2. In addition, overexpression of EHD2, without overexpression of caveolin1, resulted in loss and distortion of endogenous surface caveolae. This indicates that without the restraints of other proteins and ATP hydrolysis, the membrane-sculpting activity of EHD2 affects caveolar morphology. However, we found no effect on caveolar morphology following EHD2 depletion, suggesting that EHD2 is not essential for shaping caveolae.

EHD2 specifically associates with cell surface–connected caveolae. Such structures are formed even in the absence of EHD2, indicating that EHD2 is not required for the generation of caveolae, but rather is involved in stabilizing or controlling the dynamics of caveolae. We found that overexpression of EHD2 results in higher levels of overexpressed caveolin1 at the cell surface. In addition, depletion of EHD2 increased the number of internalized caveolae, supporting a stabilizing role of EHD2 at the plasma membrane. Caveolae can be endocytosed, but these structures appear to be very stable when compared with other invaginations, such as clathrin-coated pits (Thomsen *et al.*, 2002; Hommelgaard *et al.*, 2005). The nearly 1000-fold-slower nucleotide hydrolysis rate of EHD2, as compared with dynamin (Daumke *et al.*, 2007), might be optimized for the slow dynamics of caveolar turnover. Assembly of EHD2 oligomeric rings around caveolae might function as a cap to temporally control dynamin spiral formation and fission, as suggested for lamprey EHD1 in the synapse (Jakobsson *et al.*, 2011). A distinct pool of caveolae in stably expressing caveolin-GFP cells has been described to be highly dynamic (Pelkmans and Zerial, 2005; Boucrot *et al.*, 2011). These short-lived caveolae were shown to contain cavin and to have a residence time of only a few seconds at the plasma membrane. It is plausible that EHD2 is required to stabilize the kiss-and-run behavior of such caveolae. Indeed, we found that without functional EHD2, caveolin1-RFP formed numerous short-lived structures at the surface. However, expression of EHD2 constrained caveolin1-RFP into structures that were very stable spatially and temporally.

Taken together, our observations suggest that EHD2 is involved in stabilizing caveolar assemblies and regulating subsequent turnover of caveolae. EHD2 might cooperate with dynamin, which was previously shown to localize to caveolar necks and to promote caveolar fission, thereby controlling the stability of caveolae at the cell surface (Henley *et al.*, 1998; Oh *et al.*, 1998; Boucrot *et al.*, 2011). Indeed, pacsin2 and other membrane-remodeling, BAR domain–containing proteins have been shown to interact and function both with EHDs and dynamin (Braun *et al.*, 2005; Pant *et al.*, 2009; Senju *et al.*, 2011) and might coordinate the suggested functional crosstalk. While EHD2, cavin, and caveolin1 were stably associated at the membrane, pacsin2 only colocalized with a subset of these structures, indicating that the interaction between EHD2 and pacsin2 is temporally regulated and might be important for specific events in caveolar dynamics. EHD2 has also been described as binding other NPF-containing proteins, including rabenosyn-5 (Naslavsky *et al.*, 2004), prohibitin (Ande and Mishra, 2010), EHDBP1 (Guilherme *et al.*, 2004), myoferlins (Doherty *et al.*, 2008; Posey *et al.*, 2011), and epsin1/3 (Ko *et al.*, 2010). Our observation that EHD2-positive caveolae are limited in diffusion in the membrane suggests that these invaginations might be coupled to the cytoskeleton via such binding partners. Further definition of the proteome network around EHD2 will clarify its precise role at caveolae.

In summary, the presented data, together with previous work, support a model in which ATP-loaded EHD2 dimers are recruited to plasma membrane–associated caveolae to stabilize and control membrane curvature and fission of caveolae in an ATP hydrolysis–dependent manner. This novel caveolar marker provides mechanistic support for the process involved in the dynamics of such invaginations, knowledge of which is vital for our general understanding of the physiological significance of caveolae.

MATERIALS AND METHODS

Reagents and constructs

Polyclonal antibodies against full-length EHD2 were generated and affinity-purified using recombinant EHD2. Purchased antibodies were: mouse anti-myc clone 9E10 and rabbit anti-myc from Cell Signaling Technology (Danvers, MA); rabbit anti-caveolin1 (ab2910), rabbit anti-cavin1/PTRF, mouse anti-EEA1 (ab2900), and mouse anti-calnexin (ab22595) from Abcam (Cambridge, MA); mouse anti-caveolin1 clone 2234 from BD Transduction Laboratories (Franklin Lakes, NJ); mouse anti–AP-1 from Sigma-Aldrich (St. Louis, MO); mouse anti-MHC class I (w6/32) from the American Type Culture Collection (Manassas, VA); mouse anti-MPR6R and mouse anti-AP-2 (AP6) from Affinity BioReagents (Golden, CO); and rabbit anti-pacsin2 from BioSite, Mira Mesa, CA. All secondary antibodies were conjugated to Alexa Fluor 488, 546, or 647 (Invitrogen, Carlsbad, CA). cDNA constructs encoding human and mouse EHD2 and derivatives were described previously (Daumke *et al.*, 2007), except for the mutants F122A and ΔEH F122A, which were created using PCR-directed mutagenesis (Stratagene; Agilent, Santa Clara, CA). cDNAs from EHD1, EHD3, and EHD4 (a kind gift of M. Plomann, University of Cologne) were cloned into the pSKB-LNB vector for expression as N-terminal His fusions in *Escherichia coli*, and into the pEGFP-C3 vector for overexpression in eukaryotic cell culture. Constructs of GFP-tagged cavin1–4 were previously described (Bastiani *et al.*, 2009). RFP-tagged caveolin1 (14434; Tagawa *et al.*, 2005) and DSred-tagged Rab9 (12677), Rab11 (12662), and Rab7 (12680; Choudhury *et al.*, 2002) were purchased from Addgene (Cambridge, MA). GFP-flotillin was a kind gift from Ben Nichols (Laboratory of Molecular Biology, Cambridge). Stealth technology siRNA for EHD2 and Cavin1 knockdown was purchased from Invitrogen.

Human EHD2 siRNA: ACAAGAUCCGCGUGGUGCUCAACAA; mouse EHD2 siRNA: UUGAGUUUGCGGAAGGGCUUCUCUG; control siRNA: CAGCGAAUUCCCGCCCAAAUGACAA; mouse Cavin1 siRNAa: CCGCUGUCUACAAGGUGCCGCCUUU; mouse Cavin1 siRNAb: GCCGCAACUUCAAAGUCAUGAUCUA; mouse Cavin1 siRNAc: CACACGCUGGAGAAGCGCAUGAACA.

Protein purification, biochemical analysis, and ITC

EHD constructs were expressed in a BL21 (DE3) Rosetta *E. coli* strain as N-terminal His fusions and purified via affinity chromatography, as previously described (Daumke *et al.*, 2007). Pacsin2 constructs were expressed as N-terminal GST fusions, followed by a thrombin cleavage site in Rosetta DE3 cells (Modregger *et al.*, 2000). Cells were lysed in 50 mM HEPES (pH 7.5), 400 mM NaCl, 2.5 mM dithiothreitol (DTT), 1 mM Pefablock (Roth, Karlsruhe, Germany), 1 µg/ml DNAseI (Sigma) using a microfluidizer. A soluble extract, prepared

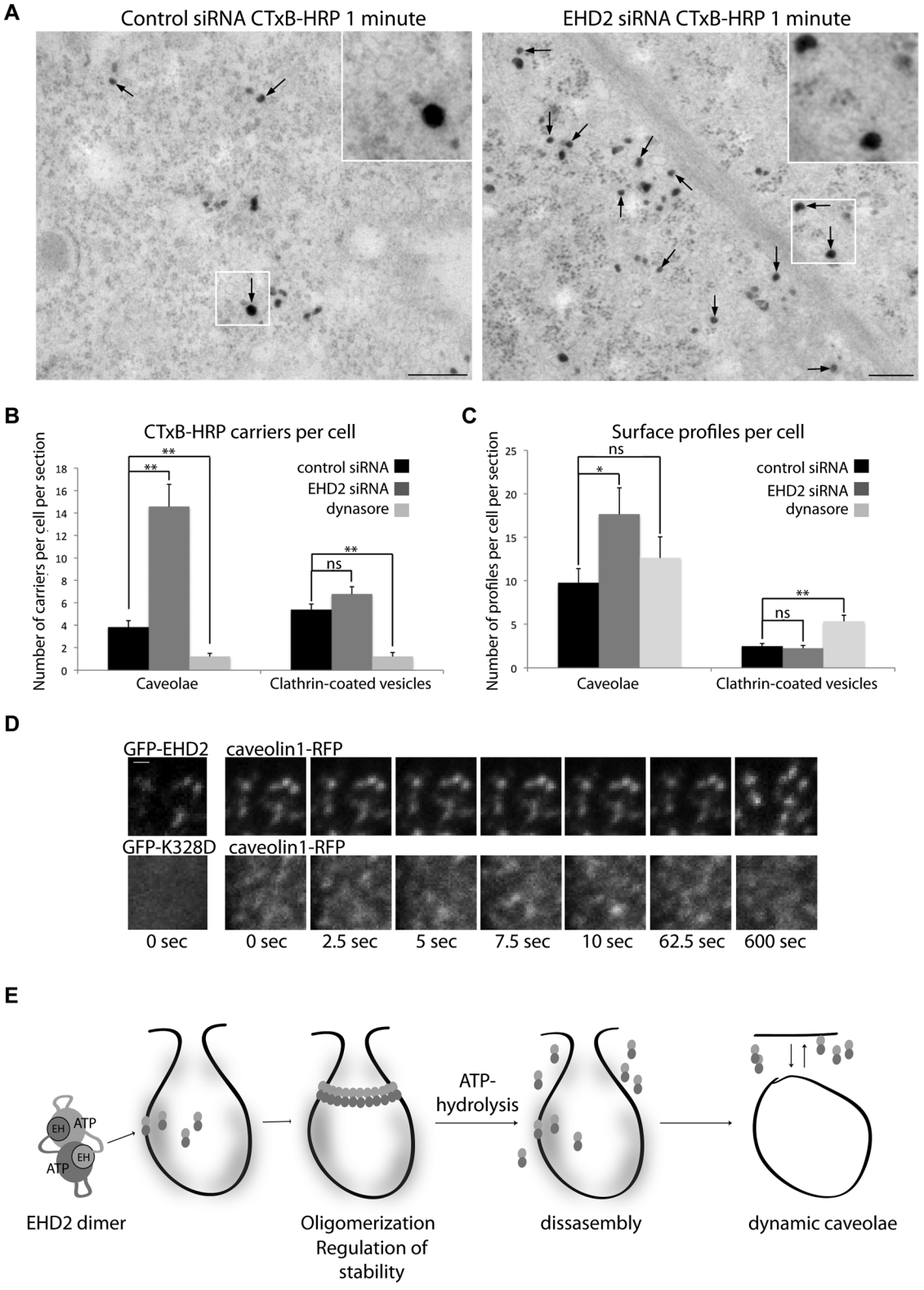

FIGURE 8: Caveolae are more dynamic in cells depleted of EHD2. (A) Representative images of 3T3-L1 cells transfected with scrambled siRNA or EHD2 siRNA and incubated with CTxB-HRP as in (B). Arrows show 55-to 75-nm, CTxB-HRP–positive budded caveolae containing the electron-dense DAB reaction product. Scale bar: 200 nm. Inset shows higher magnification of labeled and unlabeled caveolae. (B) 3T3-L1 cells were transfected with scrambled siRNA control or EHD2 siRNA, or left untransfected and treated with dynasore before addition of CTxB-HRP on ice and incubation at 37°C for 1 min. The number of electron-dense, CTxB-HRP–positive carriers was quantified per cell across 29–32 cells in three independent experiments and distinguished based on size (55–75 nm being caveolae and 80–120 nm being clathrin-coated vesicles) and morphology (caveolae being uncoated). Error bars show SEM. Two-tailed *t* tests were performed for each set of data to determine significance. ** = $p < 0.01$. (C) Ruthenium red–stained 3T3-L1 cells were

by centrifugation at 50,000 × *g* for 45 min at 4°C, was applied on a glutathione-Sepharose column, which was extensively washed with washing buffer I (20 mM HEPES, pH 7.5, 300 mM NaCl, 2.5 mM DTT) and later with 20 mM HEPES (pH 7.5), 700 mM NaCl, 2.5 mM DTT, 5 mM KH_2PO_4, 5 mM K_2HPO_4, 0.5 mM ATP, to remove Hsp70 contaminations. The GST tag was removed by addition of 500 U Thrombin (Serva, Heidelberg, Germany) in washing buffer 1 and overnight cycling at slow speed at 4°C. Cleaved protein was concentrated using ultrafiltration concentrators (molecular weight cutoff 50 kDa; Millipore, Billerica, MA) and applied on a Superdex200 26/60 gel-filtration column equilibrated with 20 mM HEPES (pH 7.5), 300 mM NaCl, 2.5 mM DTT for final purification.

To obtain lung lysates and membranes enriched for caveolae, mouse lungs were homogenized using a motor-driven glass homogenization in a HN150 (HEPES 25 mM, NaCl 150 mM) buffer supplemented with protease inhibitors. After initial centrifugation for 5 min at 800 × *g* to remove cell debris, the supernatant was centrifuged for 1 h at 60,000 rpm, and the supernatant was used as lung lysate. To obtain caveolae-enriched membranes, the pellet fraction (P1) was dissolved in HN150 supplemented with ice-cold 1% Triton X-100 for 30 min at 4°C and centrifuged for 10 min at 800 × *g*. The supernatant was adjusted to 40% sucrose, overlaid with 30 and 5% sucrose cushions, and centrifuged for 3 h at 39,000 rpm, and the 30–5% interphase was collected. The P1 pellet fraction was solubilized in HEPES 25 mM supplemented with 0.5% NP-40 and 300 mM NaCl, 1 mM DTT, and 5 mM EDTA and centrifuged at 20,000 × *g* for 20 min to obtain membrane extract. For immunoprecipitations and pull-down experiments, antibodies or proteins were coupled to tosylactivated Dynabeads (Invitrogen). Beads were incubated with the indicated lysate at 4°C for 2–4 h, washed twice in NH150 buffer with 0.1% Triton X-100 and once in NH150, boiled in sample buffer, and analyzed by SDS–PAGE and Coomassie stain or immunoblotting. For analysis of protein expression and efficiency of knockdown, 3T3-L1 or HeLa cells were lysed using 1% Triton and HN150 buffer supplemented with protease inhibitors for 30 min on ice, then centrifuged 20 min at 14,000 rpm at 4°C. Supernatants or pellets (detergent-resistant membranes) were analyzed by SDS–PAGE and immunoblotting. For analysis of total protein expression following overexpression of EHD variants, cells were sedimented, washed, and boiled directly in sample buffer before analysis by immunoblotting. For determination of cytosolic and membrane-bound fractions, control or MβCD-treated 3T3-L1 cells were harvested, washed, and frozen/thawed twice in buffer containing 25 mM HEPES, 85 mM sucrose, 1 mM MgCl, and 100 mM potassium acetate. Disrupted cells were assessed by trypan blue stain. Cells were centrifuged at 1500 rpm for 5 min, the pellet was washed and centrifuged again, and supernatants were pooled and boiled in sample buffer (cytosol). The pellet was dissolved in 1% NP40 and centrifuged at 1500 rpm for 5 min to spin down nuclei. The supernatant was centrifuged at 60,000 rpm for 1 h, and the pellet was boiled in sample buffer (total membranes). Mouse tissue lysates were generated as described above for lung lysates. ITC experiments were carried out at 10°C in a VP-ITC (MicroCal, Piscataway, NJ) in 20 mM HEPES (pH 7.5), 300 mM NaCl, 2.5 mM DTT, 2 mM $MgCl_2$, and 1 mM $CaCl_2$ at the indicated protein and ligand concentrations. Binding isotherms were fitted, and equilibrium dissociation constants were calculated using MicroCal ORIGIN software.

Cell culture, protein overexpression, and siRNA knockdown

3T3-L1 BHK, and HeLa cells were grown in DMEM medium (GIBCO, Grand Island, NY) supplemented with 10% fetal calf serum and transfected using Lipofectamine 2000 (Invitrogen) for transient protein expression. For EHD2 and cavin depletion, HeLa and 3T3-L1 cells were transfected with stealth siRNA specific against human or mouse EHD2 and cavin1, respectively, using Lipofectamine 2000 (Invitrogen), according to manufacturer's instructions. If not otherwise mentioned, 3T3-L1 cells were retransfected for optimal knockdown and supplied with fresh DMEM medium every day. Optimal knockdown was achieved after 2–3 d, as identified by SDS–PAGE and immunoblotting. Cholesterol was depleted from 3T3-L1 cells using 10 mM MβCD (Sigma-Aldrich) in DMEM medium for indicated time intervals. To observe regrowth of caveolae, cells were incubated with 10 mM MβCD in DMEM medium for 15 min and then washed out by using fresh DMEM medium and cells were incubated at 37°C, as indicated.

Immunofluorescence microscopy

For immunofluorescence analysis, HeLa and 3T3-L1 cells were fixed in 3% paraformaldehyde in phosphate-buffered saline (PBS) for 20 min at room temperature, then washed and blocked in 5% goat serum with 0.05% saponin in PBS before staining with the appropriate antibodies in 1% goat serum, 0.05% saponin in PBS using standard protocols. For immunofluorescence trafficking assays in HeLa cells, Alexa Fluor 568–conjugated transferrin (Invitrogen) was diluted in prewarmed media, added to cells, and incubated for the indicated time periods and temperatures. After washing, cells were fixed and subjected to immunofluorescence analysis, as described above. Epifluorescence images were taken using a Zeiss Axio Imager Z1 system with AxioVision software (Zeiss, Jena, Germany). For live-cell confocal microscopy, cells were grown and transfected according to standard protocols on uncoated MatTek dishes, and then placed in a temperature-controlled chamber at 37°C with 95% air/5% CO_2 and 100% humidity (Okolab, Ottaviano, Italy). Live-cell imaging data were acquired using a fully motorized inverted microscope (Nikon A1R Laser Scanning Confocal Microscope) with a 60× oil immersion lens (Plan Apochromat VC; Nikon, Tokyo, Japan) under control of the NIS-Elements microscope imaging software (Nikon). For FRAP experiments, the region of interest was photobleached for 10 s using a 488 laser. Single images were taken every 10 s before and after photobleaching, and recovery intensity was measured for a total of 10 min. TIRF microscopy was performed using a Plan Apochromat 100× oil objective lens, numerical aperture (NA) 1.49. Images were acquired with an iXon-897 electron-multiplying charge-coupled device (EMCCD) camera (Andor, Belfast, Northern Ireland).

transfected with scrambled siRNA control or EHD2 siRNA, or left untransfected and treated with dynasore. The number of ruthenium red–labeled, and thus surface-connected, caveolae and clathrin-coated vesicles (Surface profiles) were counted per cell in 30–32 cells across three independent experiments. Error bars show SEM. Two-tailed *t* tests were performed for each set of data to determine significance. * = $p < 0.05$; ** = $p < 0.01$; ns, not significant.
(D) Representative images from TIRF microscopy movie of cells cotransfected with GFP-EHD2 and caveolin-RFP or GFP-EHD2 K328 and caveolin1-RFP. Images were taken every 50 ms. Scale bars: 1 µm. (E) Proposed model for specific ATP-driven recruitment of EHD2 to caveolae via the KPF loop and subsequent oligomerization to stabilize caveolae at the surface. ATP hydrolysis–dependent disassembly of EHD2 is proposed to control oligomerization and thereby the dynamics of caveolae.

Single images were taken every 0.05 s. TIRF microscopy with combined epifluorescence microscopy experiments was performed with an Axio Observer Z1 TIRF3 system (Zeiss) with motorized TIRF-slider, using a Plan Apochromat 100× oil objective, NA 1.46. Images were acquired and analyzed by AxioVision software and a quantEM 512SC EMCCD camera (Photometrics, Tucson, AZ). Single images were taken every 0.2 s.

Electron microscopy

Samples were processed for Tokuyasu embedding and immunogold labeling using modifications of standard methods (Slot and Geuze, 2007), as described previously (Martin and Parton, 2008). Preparation and immunogold labeling of plasma membrane lawns from differentiated 3T3-L1 adipocytes were performed as described previously (Parton *et al.*, 2002). For analysis and quantification of the effect of overexpression or depletion of EHD2 on surface ultrastructure, BHK cells were transfected with GFP, GFP-EHD2, or GFP-EHD2 T94A and assayed after overnight incubation, or 3T3-L1 cells were transfected with scrambled siRNA or EHD2 siRNA, or were left untransfected and were treated with 80 μM dynasore (Sigma-Aldrich) for 30 min at 37°C. For quantification of caveolar density, BHK or 3T3-L1 cells were washed twice in PBS before fixation in 2.5% glutaraldehyde and 1 mg/ml ruthenium red for 1 h at room temperature to highlight the cell surface. Cells were washed in 0.1 M cacodylate buffer before fixation in 1% osmium tetroxide with 1 mg/ml ruthenium red for 3 h at room temperature and processed by conventional methods for Epon embedding. Ultrathin sections (55–60 nm) were cut perpendicular to the substratum (vertical sections) to give an unbiased representation of the entire plasma membrane. Quantification of surface caveolae was performed on random areas along the monolayer. Surface caveolae were defined as ruthenium red–labeled 55- to 75-nm uncoated circular profiles, as in previous studies. By these criteria, caveolae are absent from Cav1$^{-/-}$ cells. Each area was then used for quantification by moving along the monolayer in a random manner. For BHK cells, the results are from two independent transfections with four separate areas of the monolayer selected for analysis, with a total of > 45 cell profiles analyzed for each condition. For 3T3-L1 cells, the results are from three independent transfections with four separate areas of the monolayer selected for analysis, with a total of >30 cell profiles analyzed for each condition. For CTxB-HRP uptake assays, 3T3-L1 cells were transfected with scrambled siRNA or EHD2 siRNA, or were left untransfected and were treated with 80 μM dynasore (Sigma-Aldrich) for 30 min at 37°C. Cells were cooled on ice in ice-cold washing buffer (CO_2-independent media [Life Technologies, Grand Island, NY] supplemented with 1% BSA) before being bound with 10 μg/ml CTxB-HRP (Invitrogen) in ice-cold washing buffer for 30 min at 4°C. Samples were washed twice in washing buffer before incubation in prewarmed growth media (DMEM [Life Technologies]), 10% fetal bovine serum, 2 mM L-glutamine) for 1 min at 37°C. Cells were placed back on ice, washed in ice-cold washing buffer, and incubated with 1 mg/ml DAB with 50 μM ascorbic acid for 10 min. DAB solution was exchanged with DAB, ascorbic acid with 0.012% H_2O_2 for a further 20 min prior to fixation in 2.5% glutaraldehyde. Samples were processed for conventional LX112/epon (ProSciTech, Townsville, Queensland, Australia) embedded transmission electron microscopy, as previously described (Howes *et al.*, 2010).

Image and statistical analysis

For quantification of colocalization, 3–10 separate images of each condition were thresholded for the brightest areas; overlapping areas were then transferred into a new channel, and the percent colocalization area was calculated using Adobe Photoshop (San Jose, CA). To quantify the correlation of different stains, the Intensity Correlation Analysis plug-in for ImageJ was used to generate PDM (product of the differences from the mean) images and intensity correlation quotient (ICQ) correlation values. Schematic tracking of EHD2 and caveolin1 structures captured by TIRF microscopy was done manually using Adobe Photoshop. Measuring and counting of EHD2-positive tubules was done using AxioVision software. FRAP experiments were analyzed and processed using the NIS-Elements microscope imaging software. Intensity of bands identified by immunoblotting was quantified using ImageJ. Bar graphs and statistical analysis were performed using GraphPad Prism (La Jolla, CA).

ACKNOWLEDGMENTS

This work was supported by the Swedish Cancer Society; the Swedish Medical Research Council; the Swedish Foundation for Strategic Research; the Medical Faculty, Umeå University; the Magn Bergvall Foundation; the Harald Jeansson Foundation; the Åke Wiberg Foundation (R.L.); the National Health and Medical Research Council of Australia (R.G.P); and the Collaborative Research Center 740 and the Leibnitz Graduate School of Molecular Biophysics (O.D). The authors thank Robert Luetterforst for technical assistance and Michele Bastiani for performing preliminary experiments.

REFERENCES

Aboulaich N, Vainonen JP, Stralfors P, Vener AV (2004). Vectorial proteomics reveal targeting, phosphorylation and specific fragmentation of polymerase I and transcript release factor (PTRF) at the surface of caveolae in human adipocytes. Biochem J 383, 237–248.

Ande SR, Mishra S (2010). Palmitoylation of prohibitin at cysteine 69 facilitates its membrane translocation and interaction with Eps 15 homology domain protein 2 (EHD2). Biochem Cell Biol 88, 553–558.

Bastiani M, *et al.* (2009). MURC/Cavin-4 and cavin family members form tissue-specific caveolar complexes. J Cell Biol 185, 1259–1273.

Bastiani M, Parton RG (2010). Caveolae at a glance. J Cell Sci 123, 3831–3836.

Boucrot E, Howes MT, Kirchhausen T, Parton RG (2011). Redistribution of caveolae during mitosis. J Cell Sci 124, 1965–1972.

Braun A, Pinyol R, Dahlhaus R, Koch D, Fonarev P, Grant BD, Kessels MM, Qualmann B (2005). EHD proteins associate with syndapin I and II and such interactions play a crucial role in endosomal recycling. Mol Biol Cell 16, 3642–3658.

Caplan S, Naslavsky N, Hartnell LM, Lodge R, Polishchuk RS, Donaldson JG, Bonifacino JS (2002). A tubular EHD1-containing compartment involved in the recycling of major histocompatibility complex class I molecules to the plasma membrane. EMBO J 21, 2557–2567.

Choudhury A, Dominguez M, Puri V, Sharma DK, Narita K, Wheatley CL, Marks DL, Pagano RE (2002). Rab proteins mediate Golgi transport of caveola-internalized glycosphingolipids and correct lipid trafficking in Niemann-Pick C cells. J Clin Invest 109, 1541–1550.

Daumke O, Lundmark R, Vallis Y, Martens S, Butler PJ, McMahon HT (2007). Architectural and mechanistic insights into an EHD ATPase involved in membrane remodelling. Nature 449, 923–927.

Doherty KR, Demonbreun AR, Wallace GQ, Cave A, Posey AD, Heretis K, Pytel P, McNally EM (2008). The endocytic recycling protein EHD2 interacts with myoferlin to regulate myoblast fusion. J Biol Chem 283, 20252–20260.

Galperin E, Benjamin S, Rapaport D, Rotem-Yehudar R, Tolchinsky S, Horowitz M (2002). EHD3: a protein that resides in recycling tubular and vesicular membrane structures and interacts with EHD1. Traffic 3, 575–589.

George M, Ying G, Rainey MA, Solomon A, Parikh PT, Gao Q, Band V, Band H (2007). Shared as well as distinct roles of EHD proteins revealed by biochemical and functional comparisons in mammalian cells and *C. elegans*. BMC Cell Biol 8, 3.

Glebov OO, Bright NA, Nichols BJ (2006). Flotillin-1 defines a clathrin-independent endocytic pathway in mammalian cells. Nat Cell Biol 8, 46–54.

Grant B, Zhang Y, Paupard MC, Lin SX, Hall DH, Hirsh D (2001). Evidence that RME-1, a conserved *C. elegans* EH-domain protein, functions in endocytic recycling. Nat Cell Biol 3, 573–579.
Guilherme A, Soriano NA, Bose S, Holik J, Bose A, Pomerleau DP, Furcinitti P, Leszyk J, Corvera S, Czech MP (2004). EHD2 and the novel EH domain binding protein EHBP1 couple endocytosis to the actin cytoskeleton. J Biol Chem 279, 10593–10605.
Hansen CG, Bright NA, Howard G, Nichols BJ (2009). SDPR induces membrane curvature and functions in the formation of caveolae. Nat Cell Biol 11, 807–814.
Hansen CG, Howard G, Nichols BJ (2011). Pacsin 2 is recruited to caveolae and functions in caveolar biogenesis. J Cell Sci 124, 2777–2785.
Hayer A, Stoeber M, Bissig C, Helenius A (2010a). Biogenesis of caveolae: stepwise assembly of large caveolin and cavin complexes. Traffic 11, 361–382.
Hayer A, Stoeber M, Ritz D, Engel S, Meyer HH, Helenius A (2010b). Caveolin-1 is ubiquitinated and targeted to intralumenal vesicles in endolysosomes for degradation. J Cell Biol 191, 615–629.
Henley JR, Krueger EW, Oswald BJ, McNiven MA (1998). Dynamin-mediated internalization of caveolae. J Cell Biol 141, 85–99.
Hill MM *et al*. (2008). PTRF-Cavin, a conserved cytoplasmic protein required for caveola formation and function. Cell 132, 113–124.
Hommelgaard AM, Roepstorff K, Vilhardt F, Torgersen ML, Sandvig K, van Deurs B (2005). Caveolae: stable membrane domains with a potential for internalization. Traffic 6, 720–724.
Howes MT *et al*. (2010). Clathrin-independent carriers form a high capacity endocytic sorting system at the leading edge of migrating cells. J Cell Biol 190, 675–691.
Jakobsson J, Ackermann F, Andersson F, Larhammar D, Low P, Brodin L (2011). Regulation of synaptic vesicle budding and dynamin function by an EHD ATPase. J Neurosci 31, 13972–13980.
Kieken F, Sharma M, Jovic M, Giridharan SS, Naslavsky N, Caplan S, Sorgen PL (2010). Mechanism for the selective interaction of C-terminal Eps15 homology domain proteins with specific Asn-Pro-Phe-containing partners. J Biol Chem 285, 8687–8694.
Kirkham M, Fujita A, Chadda R, Nixon SJ, Kurzchalia TV, Sharma DK, Pagano RE, Hancock JF, Mayor S, Parton RG (2005). Ultrastructural identification of uncoated caveolin-independent early endocytic vehicles. J Cell Biol 168, 465–476.
Ko G, Paradise S, Chen H, Graham M, Vecchi M, Bianchi F, Cremona O, Di Fiore PP, De Camilli P (2010). Selective high-level expression of epsin 3 in gastric parietal cells, where it is localized at endocytic sites of apical canaliculi. Proc Natl Acad Sci USA 107, 21511–21516.
Lee DW, Zhao X, Scarselletta S, Schweinsberg PJ, Eisenberg E, Grant BD, Greene LE (2005). ATP binding regulates oligomerization and endosome association of RME-1 family proteins. J Biol Chem 280, 17213–17220.
Lin SX, Grant B, Hirsh D, Maxfield FR (2001). Rme-1 regulates the distribution and function of the endocytic recycling compartment in mammalian cells. Nat Cell Biol 3, 567–572.
Martin S, Parton RG (2008). Characterization of Rab18, a lipid droplet-associated small GTPase. Methods Enzymol 438, 109–129.
McMahon KA, Zajicek H, Li WP, Peyton MJ, Minna JD, Hernandez VJ, Luby-Phelps K, Anderson RG (2009). SRBC/cavin-3 is a caveolin adapter protein that regulates caveolae function. EMBO J 28, 1001–1015.
Modregger J, Ritter B, Witter B, Paulsson M, Plomann M (2000). All three PACSIN isoforms bind to endocytic proteins and inhibit endocytosis. J Cell Sci 113, 4511–4521.
Naslavsky N, Boehm M, Backlund PS, Jr., Caplan S (2004). Rabenosyn-5 and EHD1 interact and sequentially regulate protein recycling to the plasma membrane. Mol Biol Cell 15, 2410–2422.
Naslavsky N, Caplan S (2011). EHD proteins: key conductors of endocytic transport. Trends Cell Biol 21, 122–131.
Oh P, McIntosh DP, Schnitzer JE (1998). Dynamin at the neck of caveolae mediates their budding to form transport vesicles by GTP-driven fission from the plasma membrane of endothelium. J Cell Biol 141, 101–114.
Pant S, Sharma M, Patel K, Caplan S, Carr CM, Grant BD (2009). AMPH-1/Amphiphysin/Bin1 functions with RME-1/Ehd1 in endocytic recycling. Nat Cell Biol 11, 1399–1410.
Parton RG, Molero JC, Floetenmeyer M, Green KM, James DE (2002). Characterization of a distinct plasma membrane macrodomain in differentiated adipocytes. J Biol Chem 277, 46769–46778.
Parton RG, Simons K (2007). The multiple faces of caveolae. Nat Rev Mol Cell Biol 8, 185–194.
Pelkmans L, Zerial M (2005). Kinase-regulated quantal assemblies and kiss-and-run recycling of caveolae. Nature 436, 128–133.
Posey AD, Pytel P, Gardikiotes K, Demonbreun AR, Rainey M, George M, Band H, McNally EM (2011). Endocytic recycling proteins Ehd1 and Ehd2 interact with Fer-1-like-5 (Fer1l5) and mediate myoblast fusion. J Biol Chem 286, 7379–7388.
Rothberg KG, Heuser JE, Donzell WC, Ying YS, Glenney JR, Anderson RG (1992). Caveolin, a protein component of caveolae membrane coats. Cell 68, 673–682.
Senju Y, Itoh Y, Takano K, Hamada S, Suetsugu S (2011). Essential role of PACSIN2/syndapin-II in caveolae membrane sculpting. J Cell Sci 124, 2032–2040.
Sharma M, Naslavsky N, Caplan S (2008). A role for EHD4 in the regulation of early endosomal transport. Traffic 9, 995–1018.
Slot JW, Geuze HJ (2007). Cryosectioning and immunolabeling. Nat Protoc 2, 2480–2491.
Tagawa A, Mezzacasa A, Hayer A, Longatti A, Pelkmans L, Helenius A (2005). Assembly and trafficking of caveolar domains in the cell: caveolae as stable, cargo-triggered, vesicular transporters. J Cell Biol 170, 769–779.
Thomsen P, Roepstorff K, Stahlhut M, van Deurs B (2002). Caveolae are highly immobile plasma membrane microdomains, which are not involved in constitutive endocytic trafficking. Mol Biol Cell 13, 238–250.

Supplementary Information

EHD2 regulate caveola dynamics via ATP-driven targeting and oligomerization

Björn Morén[1], Claudio Shah[2], Mark T. Howes[3,] Nicole L. Schieber[3], Harvey T. McMahon[4], Robert G. Parton[3], Oliver Daumke[2], Richard Lundmark[1 §]

1 Medical Biochemistry and Biophysics, Laboratory for Molecular Infection Medicine Sweden, Umeå University, 901 87, Umeå, Sweden

2 Max-Delbrück-Centrum for Molecular Medicine, Crystallography, Robert-Rössle-Strasse 10, 13125 Berlin, Germany

3 The University of Queensland, Institute for Molecular Bioscience and Centre for Microscopy and Microanalysis, Brisbane, Australia

4 MRC Laboratory of Molecular Biology, Hills Road, Cambridge, CB2 0QH, UK

SUPPLEMENTARY FIGURES

Supplementary Figure S1

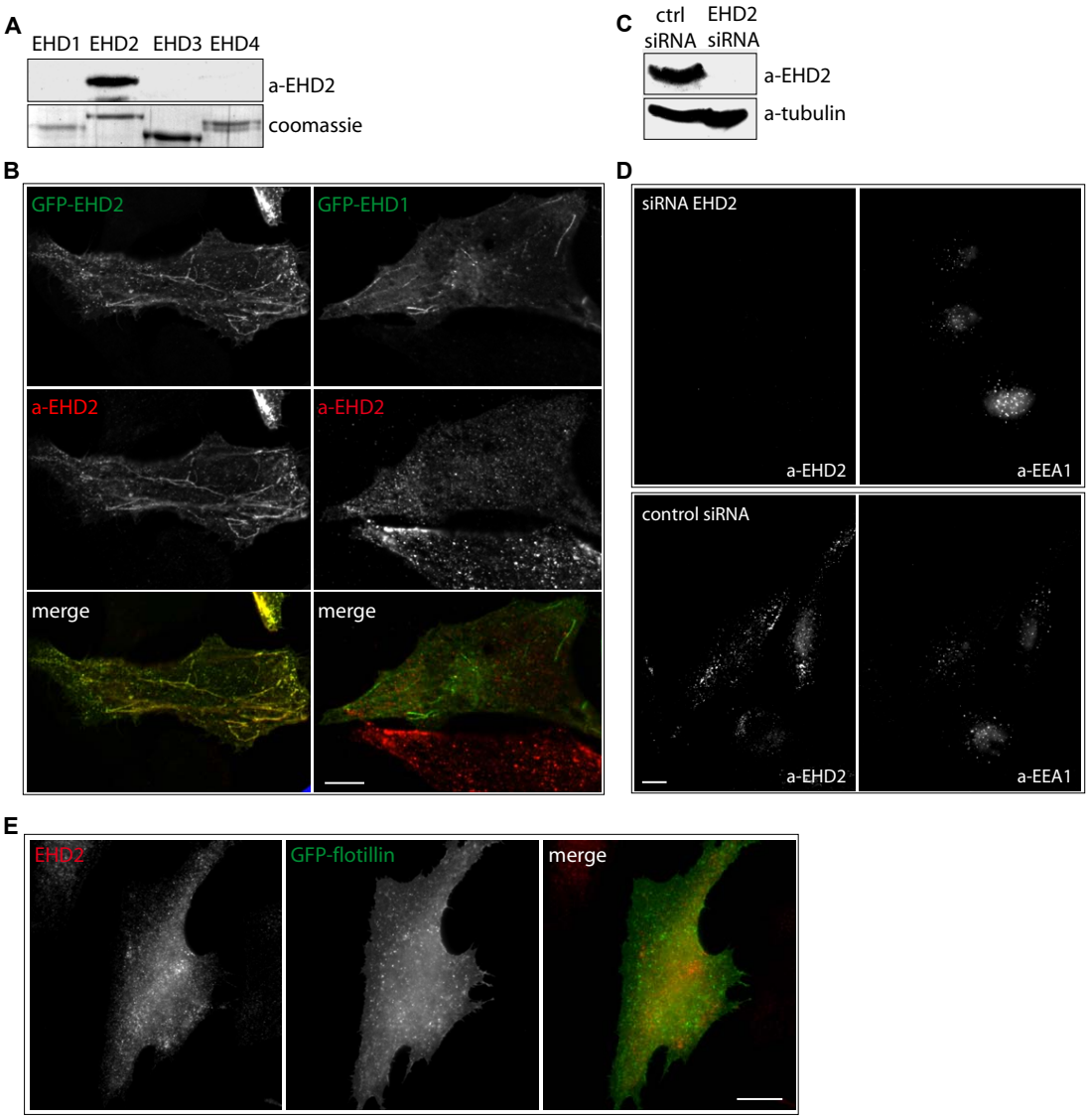

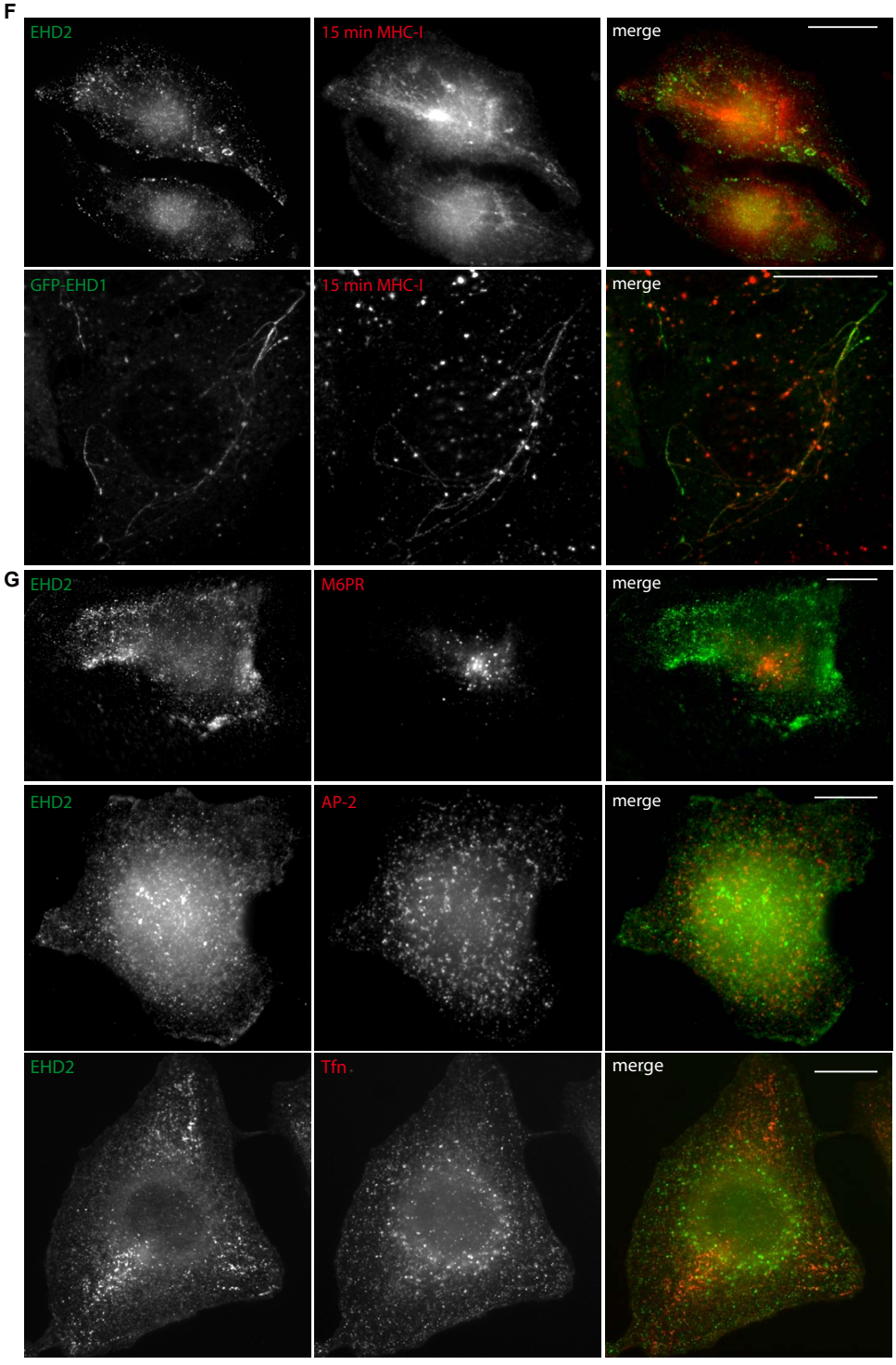
F
EHD2
15 min MHC-I
merge
GFP-EHD1
15 min MHC-I
merge
G
EHD2
M6PR
merge
EHD2
AP-2
merge
EHD2
Tfn
merge

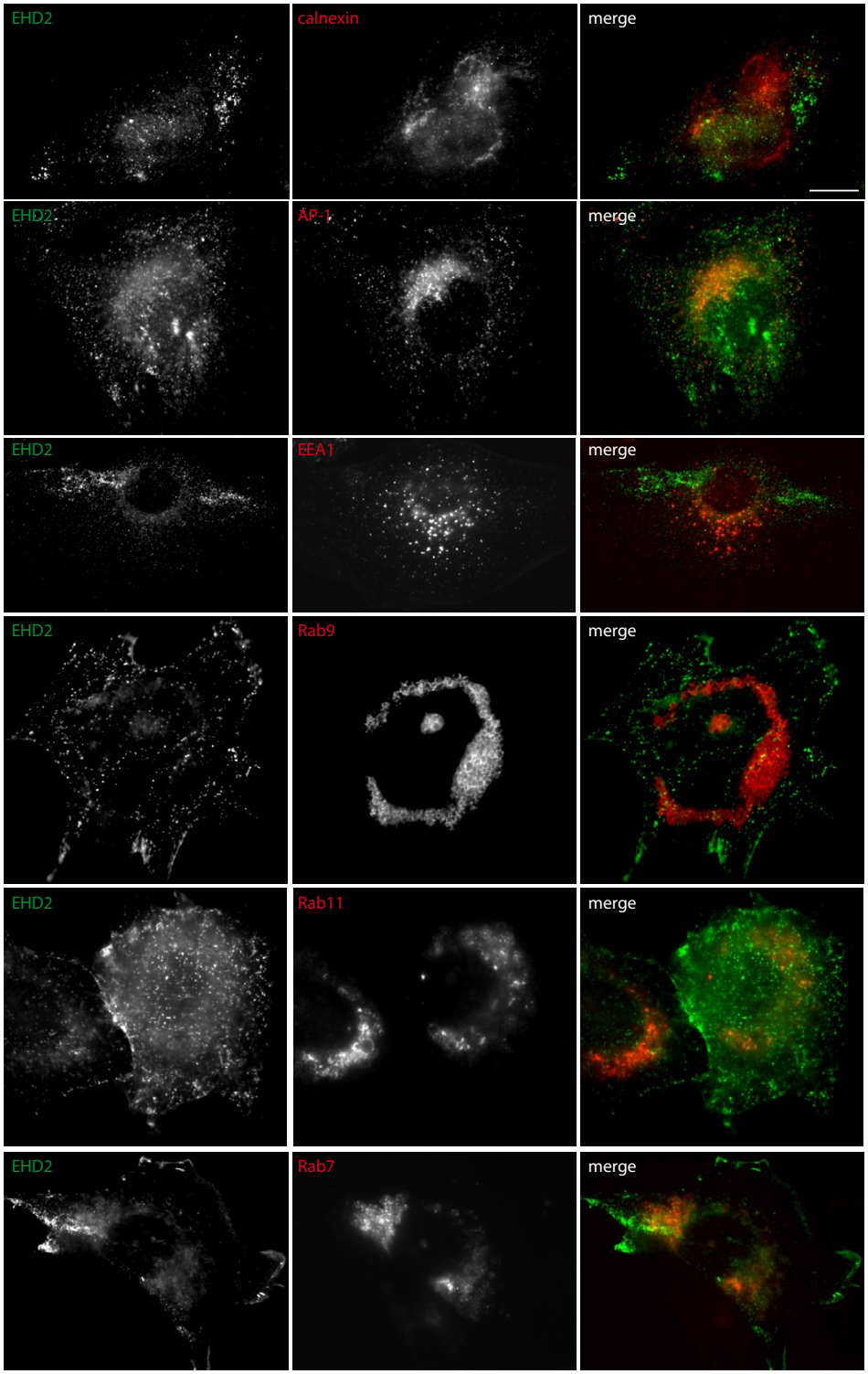

Figure S1 | Characterization of specific antibodies against EHD2. (A) Purified EHD1-4 were separated on SDS-PAGE and detected by immunoblotting using the EHD2 antibody. The lower panel shows a Coomassie stain. (B) Fluorescent micrographs of HeLa cells transfected with GFP-tagged EHD1 or EHD2 and co-labeled using EHD2-antibodies. (C-D) HeLa cells were transfected with control siRNA or siRNA specific to human EHD2 and analyzed by SDS-PAGE and immunoblotting using antibodies against EHD2 and tubulin (C), or immunofluorescent microscopy using antibodies against EHD2 and EEA1 (insets) (D).

Note that while a distinct punctate labeling pattern was detected in control cells, this labeling was ablated in siRNA-treated cells. We also noted that EHD2 was not present at EEA1-positive endosomes. (E) Representative fluorescent micrographs of HeLa cells overexpressing GFP-flotillin and co-stained for endogenous EHD2. For quantification, see Fig 1B. (F) Fluorescent micrographs showing HeLa cells that were allowed to endocytose MHC class I antibodies for 15 minutes, followed by visualization of endogenous EHD2 or GFP-EHD1 and MHC class I antibodies. (G) Panel of fluorescent micrographs of HeLa cells stained for endogenous EHD2 and co-stained for Mannose-6-phosphate receptor, or AP-2 or endocytosed transferrin (5 minutes) or markers of ER (calnexin), exit from trans-Golgi network (AP-1), early endosomes (EEA1), early to late endosomes (Rab9), recycling endosomes (Rab11) and endosomes for retrograde trafficking (Rab7). The apparent co-localization between EHD2 and Rab7 or AP-1 is due to both a diffuse cytosolic stain using the EHD2 antibody and a slight bleed-through in between channels. This co-localization is, however, not significant when analyzed by 3D confocal microscopy. Scale bars=10 μm.

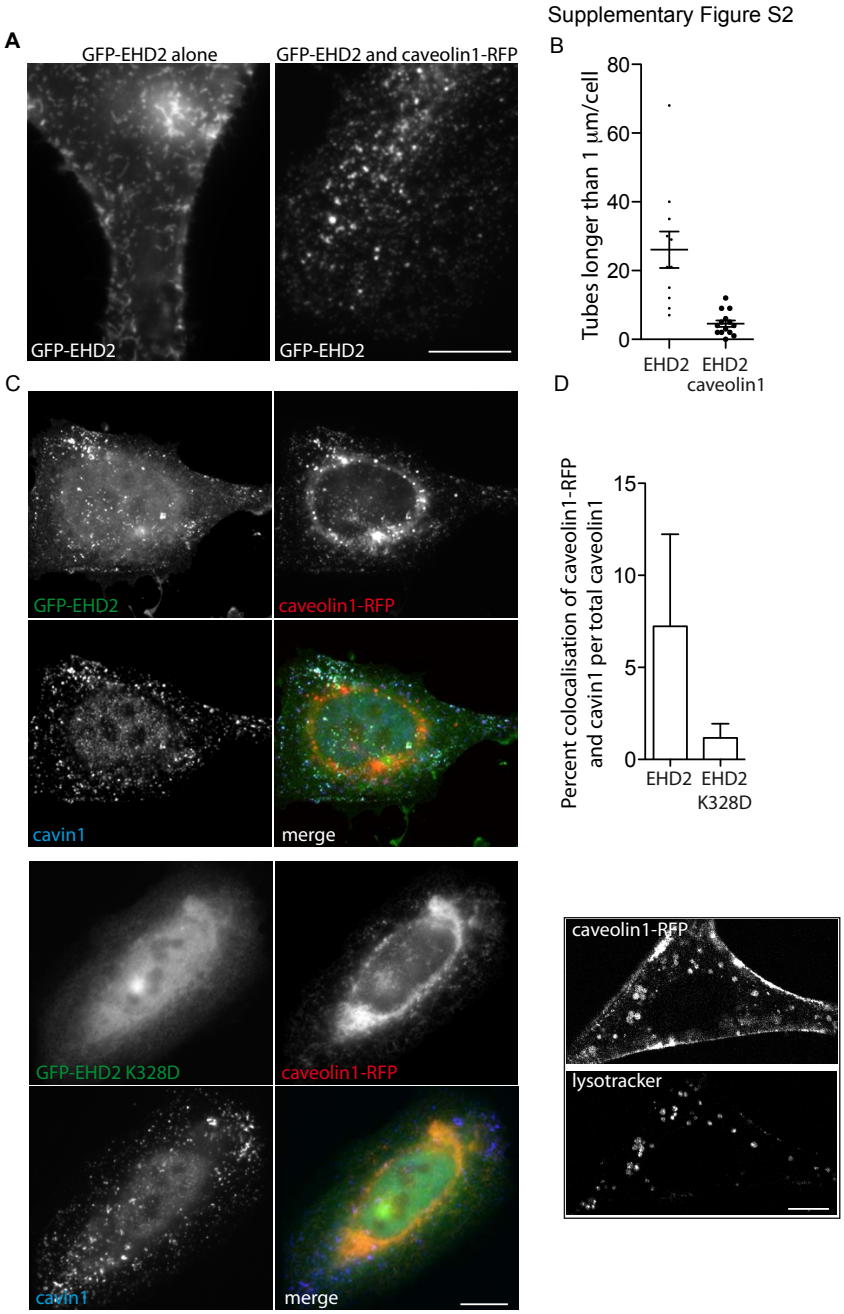

Figure S2 | Balanced expression of GFP-EHD2 and caveolin1-RFP reduces tubular localization of EHD2 and promotes localization of caveolin-RFP at the cell surface. (A) Fluorescent micrographs of HeLa cells overexpressing GPF-EHD2 alone or together with caveolin1-RFP. (B) Scatter plot showing the quantification of the number of EHD2 positive tubules longer then 1 mm per cell in cells expressing GPF-EHD2 alone or together with caveolin1-RFP. Total number of tubules was counted in 10 cells/condition. Error bars represent SEM. (C) Fluorescent micrographs of HeLa cells co-expressing GPF-EHD2 or GFP-EHD2 K328D together with caveolin1-RFP and co-stained for cavin1. (D) Bar graph showing quantification of the co-localization between caveolin1-RFP and cavin1 in cells expressing GFP-EHD2 or GFP-EHD2 K328D, as determined from 10 different cells/condition. Error bars

represent standard deviation. (E) Confocal micrograph of HeLa cell expressing caveolin1-RFP and co-stained for lysosomes using lysotracker. Scale bars=10 μm.

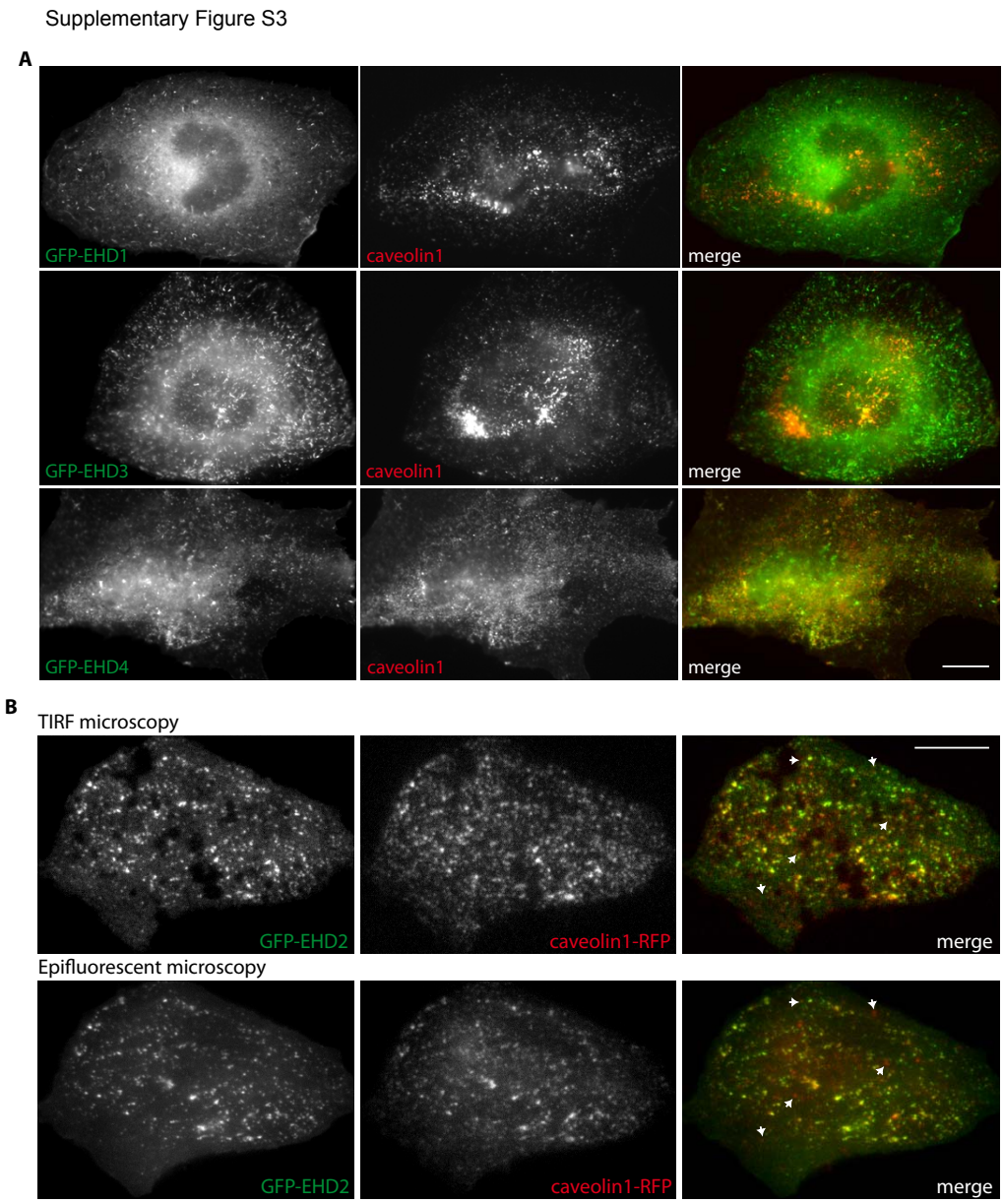

Figure S3 | EHD2, but not EHD1, EHD3 or EHD4 co-localize with caveolin1 on the cell surface. (A) Fluorescent micrographs of 3T3-L1 cells overexpressing GPF-EHD1, 3 or 4 and co-stained for caveolin1. (B) Merged and single channel fluorescent micrographs taken in epifluorescent mode (bottom panel) or TIRF mode (top panel) of a 3T3-L1 cell transfected with GFP-EHD2 and caveolin1-RFP. White arrows indicate internal caveolin1-positive structures only visible in epifluorescent mode. Note that these structures are negative for EHD2 and that EHD2 co-localize with caveolin1 structures at the cell surface. Scale bars=10 μm.

Supplementary Figure S4

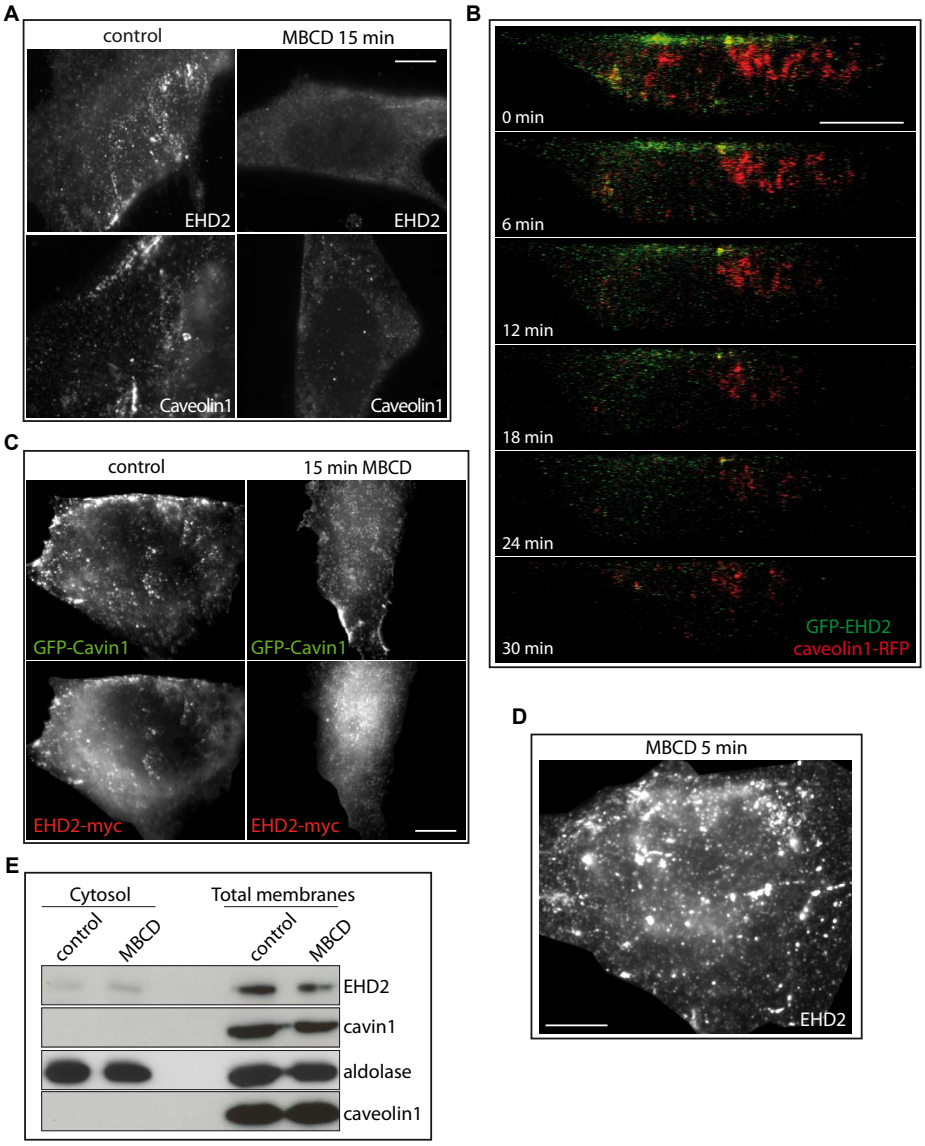

Figure S4 | Cholesterol depletion results in loss of endogenous and overexpressed EHD2 from ordered assemblies at the cell surface. (A) Fluorescent micrographs of 3T3-L1 cells treated with 15 mM MβCD for 15 minutes or PBS (control) and stained for endogenous EHD2 or caveolin1. (B) Live cell imaging of cell expressing GFP-EHD2 and RFP-caveolin1 following treatment with 15 mM MβCD. (C) Fluorescent micrographs of 3T3-L1 cells co-expressing GFP-EHD2 and RFP-cavin1 and treated with 15 mM MβCD for 15 minutes or with PBS (control). (D) Fluorescent micrographs of 3T3-L1 cells treated with 15 mM MβCD for 5 minutes and stained for endogenous EHD2. Note the tubular localization. (E) Immunoblot analysis of cytosolic and membrane-bound fractions of indicated proteins in control cells and cells treated with 15 mM MβCD for 15 minutes. Aldolase was used as a marker of

cytosolic proteins. 3T3-L1 cells were opened using freezing/thawing and cytosol was separated from total membranes by centrifugation as described. Scale bars=10 μm.

Supplementary Figure S5

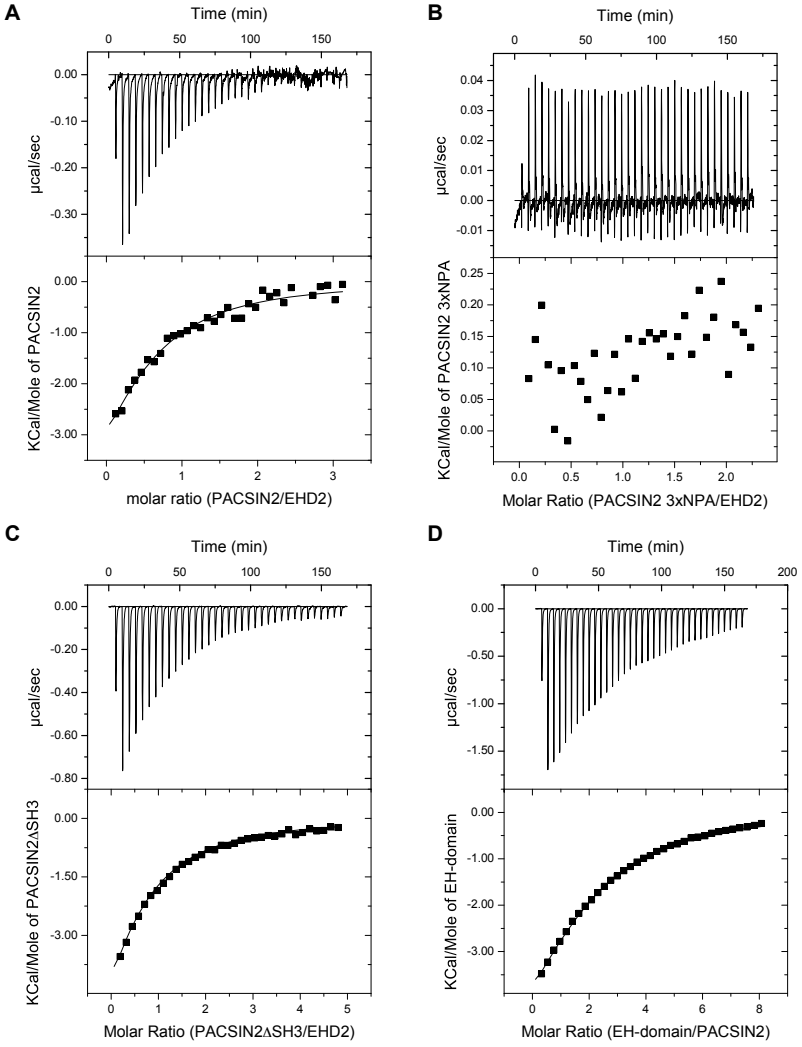

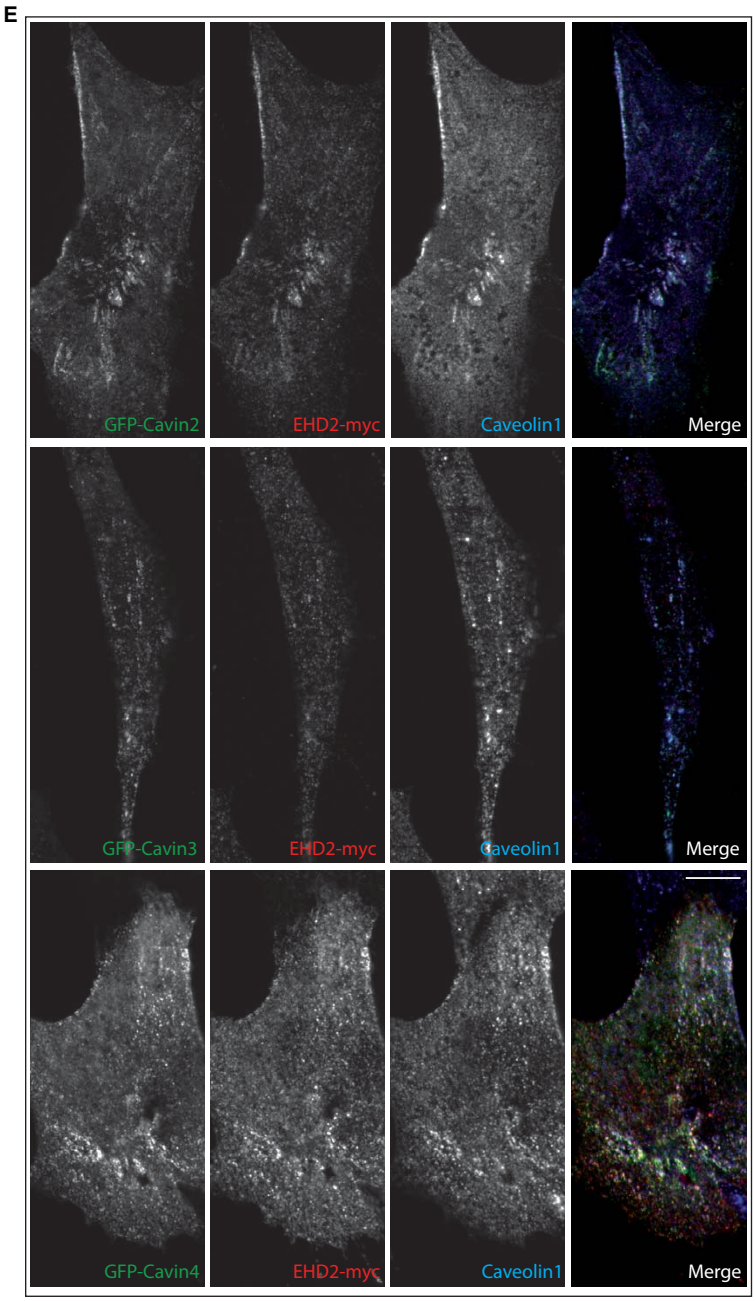

Figure S5 | Isothermal titration calorimetry and co-localization between EHD2 and cavin 2, 3 and 4. Solutions containing 0.5-1.0 mM pacsin2 wt (A), a pacsin2 variant with all three NPF motifs mutated (3xNPA) (B), or pacsin2 ΔSH3 (C) were injected stepwise into the reaction cell containing 50 μM EHD2 and the resulting heat changes were monitored. The lower panel shows the integrated heating power normalized to the concentration of injected pacsin2. The fit to the data is indicated, fitted value are shown in Figure 3F. (D) Aliquots of 2.1 mM of the isolated EH domain of EHD2 were injected stepwise into the reaction cell containing 50 μM pacsin2. (E) Fluorescent micrographs of 3T3-L1 cells co-expressing myc-EHD2 together with GFP-cavin2, GFP-cavin3 or GFP-cavin4 and co-stained for endogenous caveolin1. Scale bars=10 μm.

Supplementary Figure S6

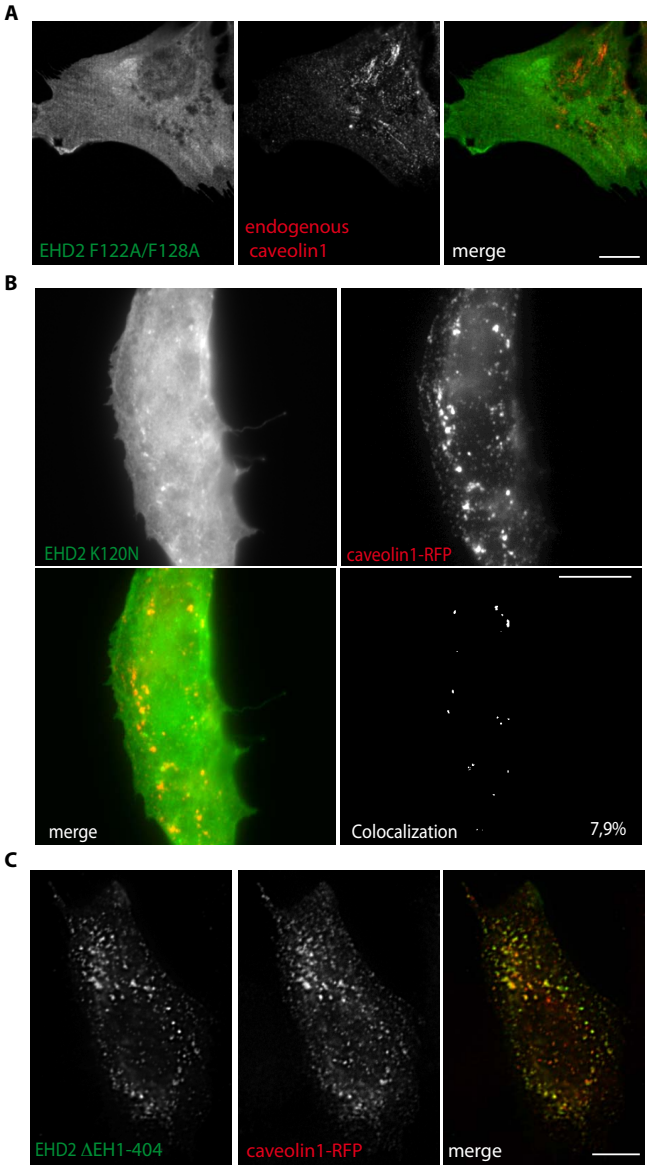

Figure S6 | EH-deletion mutants localize with caveolin1 but KPF-loop mutants affect EHD2 targeting. (A-C) Fluorescent micrographs of 3T3-L1 cells overexpressing a GFP-tagged EHD2 double mutant in the KPF loop (EHD2 F122A/F128A) (A) or a single mutant in the KPF loop (EHD2 K120N) (B) or an EH domain deletion mutant (EHD2 ΔEH_{1-404}) (C) together with caveolin1-RFP (A, C) or endogenous caveolin1 (B). Colocalizing pixels are shown to the right. The extent of co-localization was quantified as described in materials and methods. Scale bars=10μm.

Supplementary Figure S7

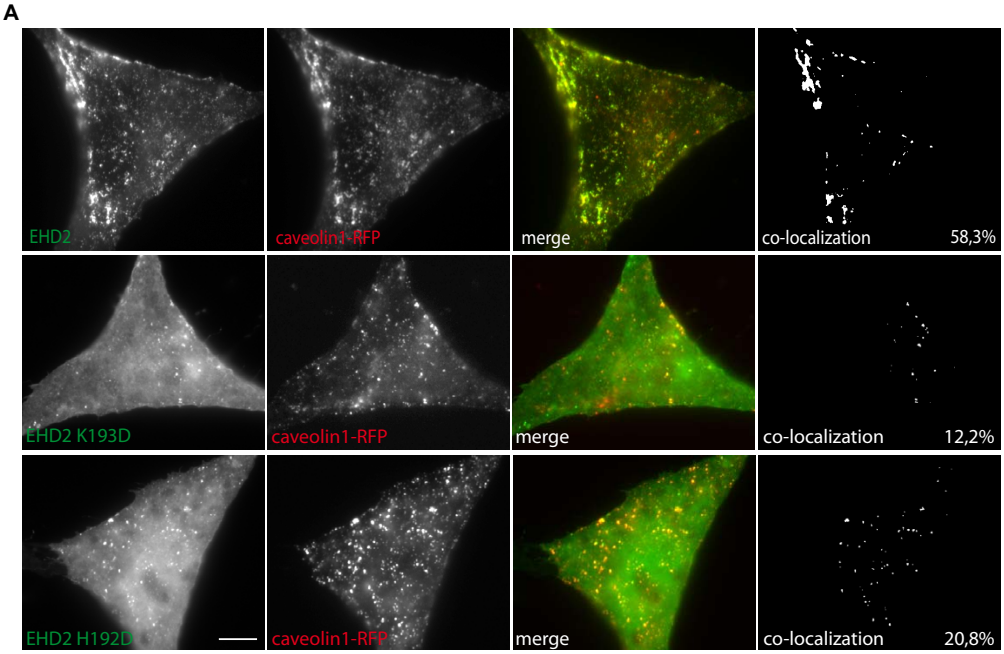

Figure S7 | ATP-hydrolysis-deficient EHD2 mutants disrupt caveolin1 structures. (A-D) Fluorescent micrographs of 3T3-L1 cells overexpressing GFP-tagged EHD2 or ATPase deficient mutants of EHD2 (EHD2 H192D and EHD2 K193D) together with caveolin1-RFP. Co-localizing pixels are shown to the right. The extent of co-localization was quantified as described in materials and methods. Scale bars=10 μm.

Movie S1 | **FRAP-microscopy movie of GFP-EHD2 and caveolin1-RFP.** Live-cell confocal microscopy movie of 3T3-L1 cell co-transfected with GFP-EHD2 and caveolin1-RFP. Images were acquired before bleaching and then every 10 seconds. The regions of interest were bleached for 10 seconds. Representative micrographs are shown in Fig 2D.

Movie S2 | **FRAP-microscopy movie of GFP-EHD2 F122A and caveolin1-RFP.** Live-cell confocal microscopy movie of 3T3-L1 cell co-transfected with GFP-EHD2 F122A and Caveolin1-RFP. Images were acquired before bleaching and then every 10 seconds. The regions of interest were bleached for 10 seconds. Representative micrographs are shown in Fig 4F.

Movie S3 | **Caveolin1-RFP is highly dynamic on the cell surface in GFP-EHD2 K328D expressing cells.** (A-B) Movies of cell co-transfected with GFP-EHD2 K328D and Cav1-RFP acquired by live-cell TIRF-microscopy and presented in red and green channels (A) or only the red channel for visualizing caveolin1-RFP dynamics (B). Images were taken every 50 milliseconds as described. Representative micrographs are shown in Fig 8D.

Movie S4 | **GFP-EHD2 and caveolin1-RFP positive caveolae are stably associated with the cell surface** (A-B) Movies of cell co-transfected with GFP-EHD2 and Cav1-RFP acquired by live-cell TIRF-microscopy and presented in red and green channels (A) or only the red channel for visualizing caveolin1-RFP dynamics (B). Images were taken every 50 milliseconds as described. Representative micrographs are shown in Fig 8D.